UniCon: Unidirectional Information Flow for Effective Control of Large-Scale Diffusion Models

Anonymous authors
Paper under double-blind review

Abstract

We introduce UniCon, a novel architecture designed to enhance control and efficiency in training adapters for large-scale diffusion models like the Diffusion transformer. Unlike existing methods that rely on bidirectional interaction between the diffusion model and control adapter, UniCon implements a unidirectional flow from the diffusion network to the adapter, allowing the adapter alone to generate the final output. UniCon reduces computational demands by eliminating the need for the diffusion model to compute and store gradients during adapter training. UniCon is free from the constrains of encoder-focused designs and is able to utilize all parameters of the diffusion model, making it highly effective for transformer-based architectures. Our results indicate that UniCon reduces GPU memory usage by one-third and increases training speed by 2.3 times, while all maintaining the same adapter parameter size. Additionally, without requiring extra computational resources, UniCon enables the training of adapters with double the parameter volume of existing ControlNets. In a series of image condition generation tasks, UniCon has demonstrated precise response to control information and excellent generation capabilities. UniCon makes the control of large-scale diffusion models feasible and provides a basis for further scaling up of diffusion models.

1 Introduction

Diffusion generative models (Ho et al., 2020; Song et al., 2020; Nichol & Dhariwal, 2021; Rombach et al., 2022), with their exceptional generative effects and diversity, have significantly impacted computer vision fields, such as creative design (Anciukevičius et al., 2023; Mittal et al., 2021; Cao et al., 2024), image processing (Wang et al., 2023b; Lin et al., 2023; Yang et al., 2023; Yu et al., 2024), and personalized content generation (Zhang et al., 2023; Mou et al., 2024; Li et al., 2024; 2023b; Zhao et al., 2024). This is particularly due to their ability to precisely control complex layouts, poses, shapes, and image conditions through both textual and visual prompts. These functions typically require training an additional adapter or controller network associated with the diffusion model, enabling control of the output during the inference process (Zhang et al., 2023; Mou et al., 2024; Zavadski et al., 2023; Zhao et al., 2024). The most successful representative is ControlNet (Zhang et al., 2023) for Stable Diffusion (SD) (Rombach et al., 2022), which includes a trainable copy of the SD U-Net encoder part and zero convolutions as connectors. To achieve higher quality generation and more precise control, the parameter size of diffusion models has also been significantly increased (Podell et al., 2023; Lin et al., 2024; Sauer et al., 2023). Starting from the original SD model (Rombach et al., 2022) with 0.86 billion parameters, the advanced SDXL (Podell et al., 2023) has scaled up to 2.6 billion parameters. The latest models (Peebles & Xie, 2023; Bao et al., 2023) even replaced the commonly-used U-Net architecture with transformer-based models to obtain better property. The benefits of scaling up have not yet reached their limit. We may expect larger diffusion models and advanced transformer architectures to appear in the future (Xie et al., 2023; Han et al., 2023; Luo et al., 2023; Chen et al., 2024a). Under this trend, the limitations of existing control adapters for diffusion models have become increasingly apparent.

There are three main problems: First, as the parameters of the diffusion model increase, the size of its adapter also needs to be expanded accordingly (Zhang et al., 2023). Existing adapters not

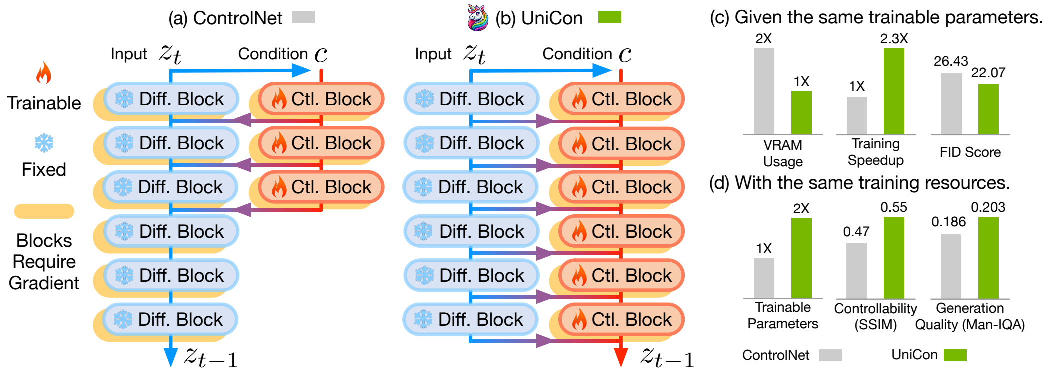

Figure 1: This figure illustrates the schematic comparison between our proposed UniCon and ControlNet. In UniCon, information flows unidirectionally from the diffusion model to the adapter network, which directly outputs the results. This design is highly computationally efficient as it does not require computing and storing gradients for the diffusion model. (c) displays results generated from downsampled images, and (d) shows outcomes based on depth maps. UniCon achieves improved performance while utilizing fewer resources.

only need to calculate their own gradients for training, but also have to calculate and store the gradients of the diffusion model, placing significant strain on computational resources Mou et al. (2024); Zavadski et al. (2023). This typically implies nearly double the additional overhead. Second, while existing adapter designs exert control by modifying features in intermediate layers, they still process these modified features using the original parameters of the diffusion model. The generative capabilities of models with fixed parameters are limited when only the intermediate features are modified. Third, the design of existing control adapters assumes that the diffusion models use an encoder-decoder architecture (*i.e.* U-Net), which is inadequate for transformer-based diffusion models due to their inability to separate encoder and decoder components. Since existing adapters primarily implement control within the encoder part, their response to control signals lacks pixel-level precision, particularly problematic in high-precision tasks such as image restoration based on low-quality images.

In this paper, we introduce a novel design specifically tailored for training control adapters for the next generation of large-scale diffusion models, such as DiT. This design facilitates further scaling up of diffusion models and their control. Unlike the existing methods (Zhang et al., 2023; Zavadski et al., 2023) that use adapters to intervene during the forward inference of diffusion models in a bidirectional manner, our approach allows information to flow unidirectionally from the diffusion network to the adapter, without flowing backward. The final output image will be generated by the adapter, NOT the diffusion model. Our method is therefore called UniCon. Figure 1 illustrates the design difference of UniCon and ControlNet. The advantage of UniCon is that during training, the diffusion model only needs to perform forward propagation and does not need to compute or store gradients. Additionally, UniCon can utilize all parameters and architectures of the diffusion model, not just those pertaining to the encoder, making it entirely suitable for diffusion models with large scale transformer architecture. Moreover, since the output processing is handled by the adapter, our design enables more precise control over generation based on conditions. UniCon avoids micro-interventions in the diffusion model architecture, thus could further enhance the versatility.

We test the UniCon architecture across a variety of conditional generative tasks, validating it on both the SD U-Net diffusion model and the DiT diffusion model. Notably, when applying UniCon adapter to the transformer-based DiT diffusion model, our approach saves half of the video memory (VRAM) usage while achieving a 2.3X increase in training speed, without increasing the adapter's parameter size. It also delivers superior FID scores and condition fidelity in tasks involving image generation from downsampled images, see Figure 1 (c). By employing our method in the generation task according to canny edge, the parameter size of the adapter can be doubled without additional computational resources. UniCon can further improve performance, where our method not only enhances the quality of generation but also ensures optimal controllability.

2 RELATED WORK

Diffusion generative models. The diffusion models (Sohl-Dickstein et al., 2015) have been explored across a variety of generative tasks, such as image-to-image translation (Saharia et al., 2022a; Zhao et al., 2022; Li et al., 2023a), text-to-image synthesis (Rombach et al., 2022; Saharia et al., 2022b; Avrahami et al., 2022; Jiang et al., 2022), image restoration (Saharia et al., 2022c; Daniels et al., 2021; Kawar et al., 2022; Lin et al., 2023; Yu et al., 2024), image editing (Meng et al., 2021; Avrahami et al., 2022; 2023), image inpainting (Nichol et al., 2021; Lugmayr et al., 2022), etc. Among them, some text-to-image diffusion models are also used as foundation models. Their capabilities can be applied to many downstream tasks. Model up has been an important means to improve the capabilities of these foundation models, and a lot of efforts have been made, *e.g.*a series of works proposed by the Stability AI, including SD-2.1 (Rombach et al., 2022), SD-XL (Podell et al., 2023), SD-Cascade (Pernias et al., 2023), and SD3 (Esser et al., 2024). In order to further expand and improve the capacity of the model, the large-scale transformer architecture is also introduced into the diffusion models, including DiT (Peebles & Xie, 2023), U-ViT (Bao et al., 2023), SD3 (Esser et al., 2024) and the PixArt family (Chen et al., 2023; 2024b;a).

Controlled generation of diffusion models. Pre-trained large-scale diffusion models serve as foundational models that can be fine-tuned for a variety of downstream tasks. The fine-tuning process should be designed to mitigate issues such as overfitting, model collapse, and catastrophic forgetting. Various fine-tuning methods have been developed across multiple fields, including HyperNetworks (Alaluf et al., 2022; Dinh et al., 2022), additive learning (Rosenfeld & Tsotsos, 2018; Mallya et al., 2018; Mallya & Lazebnik, 2018; Serra et al., 2018), and Low-Rank Adaptation (LoRA) (Hu et al., 2021). For diffusion foundation models, the most effective and commonly used approach for enhancing generation quality and controllability involves training an additional adapter network (Houlsby et al., 2019; Stickland & Murray, 2019; Li et al., 2022; Mou et al., 2024; Ju et al., 2024; Mo et al., 2023). Zhang *et al.* (Zhang et al., 2023) first introduced ControlNet, an architecture designed to incorporate spatial conditioning controls into large, pre-trained diffusion models. The ControlNet is connected with zero-initialized convolution layers that progressively grow the parameters from zero and ensure that no harmful noise could affect the fine-tuning. Building on this, ControlNet-XS (Denis Zavadski & Rother, 2023) explored different sizes and architectural designs of ControlNet to enhance control over the image generation process in stable diffusion-based models. Additionally, T2I-Adapter (Mou et al., 2024) focused on aligning internal knowledge within T2I models with external control signals, while keeping the original large T2I models unchanged. This approach allows for the training of various adapters under different conditions, such as text and image, to achieve detailed control and editing capabilities in the color and structure of the generated images. Uni-ControlNet (Zhao et al., 2024) integrates various local and global controls into a single model, using only two additional adapters for fine-tuning on pre-trained text-to-image diffusion models, thus avoiding the extensive costs of training from scratch. Furthermore, surpassing existing diffusion-based restoration methods (Wang et al., 2023b; Lin et al., 2023; Yang et al., 2023), SUPIR (Yu et al., 2024) leverages the generative prior and the potential of model to enable photo-realistic restoration of severely degraded images through textual prompts. This illustrates the significant potential of diffusion models in enhancing image quality and fidelity in controlled generation tasks.

3 METHOD

Preliminary and motivation. A typical diffusion model involves two processes: a forward process that gradually adds a small amount of noise to the image, and a corresponding backward denoising process that recovers the input image by gradually removing the noise. Given a pre-trained diffusion model $\mathcal{H}(\cdot)$, it can either have a U-Net-like structure, as in SD, or a transformer structure, as in the DiT model. When performing the backward generation process, the diffusion model takes the last denoised result z_t and time step t as well as the text prompt p as input, and predicts the next result of denoising generation $z_{t-1} = \mathcal{H}(z_t, t, p)$. The existing adapters directly modify the features X_h of the intermediate layer of $\mathcal{H}$ during the denoising generation process to modify the generation results according to conditions. Assume we have an adapter $\mathcal{C}(\cdot)$, usually it may take z_t, t and p as inputs. Additionally, it may also take X_h as inputs (Zavadski et al., 2023). The output of the adapter $\mathcal{C}$ is a series of residual modified values X_c of the intermediate layers X_h. In ControlNet, X_c will be

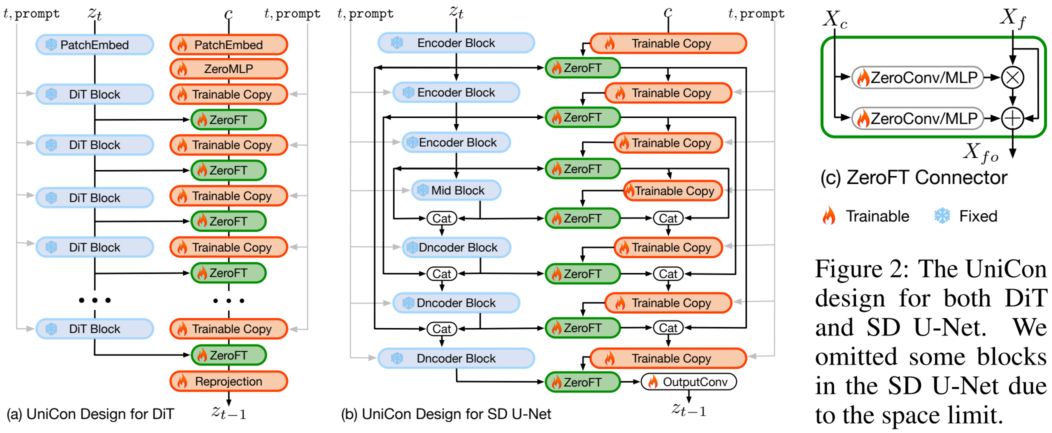

(a) UniCon Design for DiT

(b) UniCon Design for SD U-Net

(c) ZeroFT Connector

Figure 2: The UniCon design for both DiT and SD U-Net. We omitted some blocks in the SD U-Net due to the space limit.

directly added to the corresponding intermediate layer of $\mathcal{H}$ using element-wised addition to generate a new representation $X_h' = X_c + X_h$ to implement conditional generation.

This intuitive paradigm aligns with the common practice of fine-tuning large pre-trained diffusion models, yet it introduces several significant issues:

Firstly, this approach directly impacts the diffusion model; therefore, training the adapter involves calculating the gradients of the modified diffusion model and subsequently backpropagating these gradients to the adapter's trainable parameters. To achieve rapid and stable convergence, the adapter's initial parameters are generally set as a trainable copy of the diffusion model. This can lead to training costs for the adapter surpassing those of the diffusion model itself. For example, when training ControlNet for DiT, when the gradient of ControlNet itself occupies about 18GB VRAM, the gradient brought by the DiT diffusion model needs to occupy 16GB VRAM, and this cost can be optimized. As the parameter number and resource demands of diffusion models escalate, training large adapters for large-scale models presents significant engineering challenges.

Secondly, while modifying the features of intermediate layers can directly alter the output, this technique still depends on pre-trained parameters to process these changes. When parameters are fixed, adapting the model to new data by only changing the input of each layer restricts its generative capabilities. Alternative methods such as LoRA (Hu et al., 2021) or full-parameter fine-tuning permit direct modifications of parameters but also come with limitations. LoRA is constrained by its scale, and full-parameter tuning risks losing previously learned generative capabilities.

Finally, the existing design of control adapters, which often assumes a U-Net-like encoder-decoder diffusion architecture (Zhang et al., 2023; Mou et al., 2024; Zavadski et al., 2023; Zhao et al., 2024) and focuses primarily on the encoder (Zhang et al., 2023), does not suit for transformer-based diffusion models. This mismatch arises because it is difficult to distinctly separate the encoder and decoder components in such models. Indiscriminately controlling the entire transformer model escalates resource demands due to the necessity of computing and storing the diffusion model's gradients. Furthermore, since existing adapters mainly focus on the encoder, their response to control signals lacks pixel-level precision, particularly problematic in high-precision tasks such as generation based on low-quality images.

Unidirectional information flow design paradigm. We propose a design paradigm named UniCon to address these issues. For a clearer understanding, readers are encouraged to refer to Figure1. Our approach ensures that the pre-trained diffusion model $\mathcal{H}$ is used only for inference, thereby eliminating the need to compute and store its gradients. Information flows unidirectionally from $\mathcal{H}$ to the UniCon adapter $\mathcal{C}_{UC}$, positioning the adapter as a trainable decoder that processes information from the diffusion model's layers. Specifically, denote $X_h = x_{h1}, x_{h2}, \ldots$ as the outputs from the intermediate layers of $\mathcal{H}$. The UniCon adapter receives these intermediate features along with the inputs of the condition c, time step t, and prompt p. The output of the adapter under this step is the denoising result $z_{t-1} = \mathcal{C}_{UC}(c, t, p, X_h)$. This design establishes a unidirectional information flow path from $z_t \rightarrow \mathcal{H}(\cdot) \rightarrow X_h \rightarrow \mathcal{C}_{UC}(\cdot) \rightarrow z_{t-1}$, ensuring that information does not revert to the

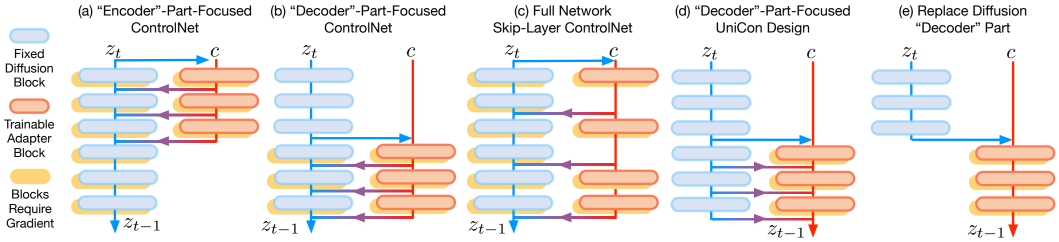
(a) "Encoder"-Part-Focused ControlNet
(b) "Decoder"-Part-Focused ControlNet
(c) Full Network Skip-Layer ControlNet
(d) "Decoder"-Part-Focused UniCon Design
(e) Replace Diffusion "Decoder" Part
Fixed Diffusion Block
Trainable Adapter Block
Blocks Require Gradient
z_t
c
z_{t-1}

Figure 3: Schematic representation of the five different variants we covered in our ablation studies.

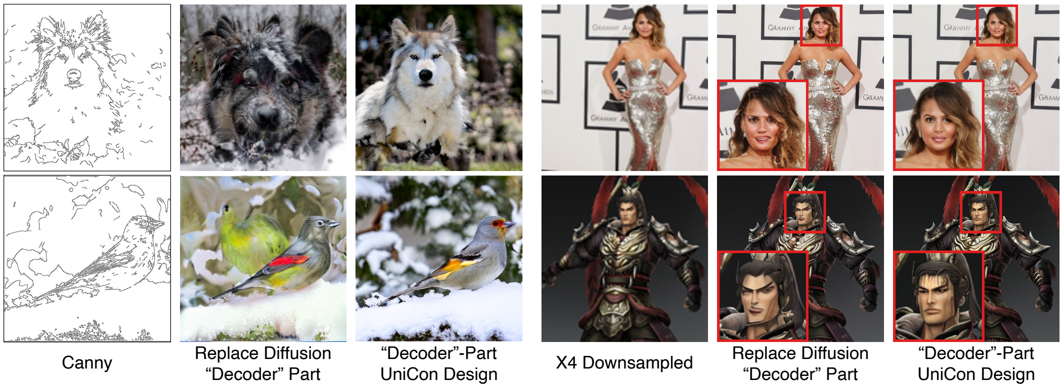
Canny
Replace Diffusion "Decoder" Part
"Decoder"-Part UniCon Design
X4 Downsampled
Replace Diffusion "Decoder" Part
"Decoder"-Part UniCon Design

Figure 4: The comparison between decoder-part-focused UniCon and replace diffusion decoder part. The results indicate that if the complete pre-trained diffusion model is not preserved, there is a significant decline in generative capabilities. These two models are shown in Figure 3 (d) and (e).

pre-trained diffusion model. By mirroring the architecture and parameters of the diffusion model in the adapter and using a zero-initialized connector for integration, we can ensure stable training.

This design resolves issues found in existing approaches. Firstly, the diffusion model only participates in forward inference, eliminating the need for computing and storing its gradients, which significantly reduces computational costs. Secondly, all adapter parameters are trainable, and the adapter directly delivers processed outputs, bypassing the fixed parameters of the diffusion model. At the same time, the well-trained diffusion model remains unchanged, ensuring the generative capabilities are less likely to be forgotten during fine-tuning. This enhances the generative capabilities and leads to improved generation quality. Moreover, as there is no need to intervene in the diffusion model – only to extract the computed features from intermediate layers – our solution is highly adaptable to different diffusion architectures, from U-Net to transformer model with ease. Finally, the adapter no longer relies solely on the encoder or parts of the diffusion model but instead produces the output directly, further improving the preservation of control signals in tasks requiring high precision.

The proposed UniCon adapter designs. In this work, we use DiT and SD U-Net to validate our UniCon adapter paradigm. Nevertheless, we note that the UniCon design paradigm is widely applicable and can be employed across various diffusion models. Figure2(a) and Figure2(b) show the structural details when UniCon is applied to DiT and SD U-Net. The design of the UniCon adapter, applicable to both DiT and U-Net models, starts with a trainable copy that includes all parameters and architectures of the diffusion model. In order to connect the diffusion model to the adapter, a connector module is also required. For each output x_h of a DiT block or U-Net block, it introduces information from x_h to the corresponding location in the adapter. Zero-initialized convolutional layers (ZeroConv) or fully connected layers (ZeroMLP) are simple and stable choices for U-Net and DiT. This approach prevents unwanted noise from affecting features in trainable replicas at the beginning of training. We additionally propose here a new connector called Zero-initialization Feature Transform (ZeroFT). ZeroFT not only utilizes element-wise addition but also incorporates element-wise multiplication and a shortcut connection, enhancing the integration and transfer of information. This setup is detailed in Figure2(c). The parameters in both two layers within ZeroFT – whether convolutional or fully-connected layers – are initialized to zero. According to our experiments, ZeroFT is more effective than ZeroMLP/Conv in generating effects and controlling performance.

Task	ControlNet Size	Controllability↑	FID↓	Clip-Score↑
Canny (SSIM)	Encoder	0.4748	51.52	0.7724
	Decoder	**0.5131**	59.32	0.7507
	Skip-Layer	0.4983	**49.78**	0.7776
	Full	0.5053	50.17	**0.7818**
SR (PSNR)	Encoder	34.82	26.43	0.7996
	Decoder	34.85	25.84	0.8013
	Skip-Layer	35.49	24.99	0.8009
	Full	**36.53**	**23.04**	**0.8026**

(a) The results of copy different parts in ControlNet.

Task	Connector Type	Controllability↑	FID↓	Clip-Score↑
Canny (SSIM)	ZeroMLP	0.5343	55.22	0.7612
	ShareAttn	0.5236	56.22	0.7606
	ZeroFT	**0.5426**	**52.31**	**0.7696**
SR (PSNR)	ZeroMLP	**35.67**	22.99	0.8013
	ShareAttn	35.55	23.03	0.8012
	ZeroFT	35.64	**22.07**	**0.8025**

(b) The results of different connector designs used in the UniCon Adapter.

Task	Adapter	Unidirectional	Controllability↑	Generation Quality				Text Consistency
				FID↓	Clip-IQA↑	MAN-IQA↑	MUSIQ↑	Clip-Score↑
Canny (SSIM)	Skip-Layer	✗	0.4983	**49.78**	**0.6629**	**0.1978**	**66.05**	**0.7776**
		✓	**0.5078**	56.93	0.6224	0.1737	63.66	0.7561
	Decoder	✗	0.5131	59.32	0.6047	0.1621	62.51	0.7507
		✓	**0.5343**	**55.22**	**0.6347**	**0.1780**	**64.27**	**0.7612**
	Full	✗	0.5053	50.17	0.6397	0.1867	64.70	0.7818
		✓	**0.5458**	**46.71**	**0.6577**	**0.2029**	**66.45**	**0.7889**
SR (PSNR)	Decoder	✗	34.85	25.84	0.6979	0.2325	68.26	0.8013
		✓	**35.59**	**23.55**	**0.7036**	**0.2358**	**68.61**	**0.8018**
	Full	✗	36.53	23.04	0.7212	0.2609	69.91	**0.8026**
		✓	**37.34**	**20.34**	**0.7251**	**0.2831**	**69.99**	0.8022

(c) The effect of the proposed unidirectional information flow design.

Table 1: Ablation study of different adapter designs. The diffusion model used in these experiments is DiT transformer-based model. ↑ indicates the larger the better and ↓ indicates the lower the better.

4 EXPERIMENTS

4.1 EXPERIMENT SETTINGS

Tasks and datasets. We employ five different conditions image generation for testing: canny edge (Canny, 1986), depth maps (Ranftl et al., 2021), OpenPose (Cao et al., 2019), 4× downsampling (SR) (Wang et al., 2018), and blurring (sigma=2) followed by 4x downsampling (deblur+downsampling) (Kong et al., 2022; Yu et al., 2024). These conditions can broadly be classified into two categories: (1) tasks that require the model to generate high-level semantic content, such as OpenPose, depth maps, and canny edge, which we refer as high-level control generation tasks; and (2) tasks that emphasize local generation and require higher precision in control, such as 4× downsampling and bluring+downsampling, which we call low-level control generation. The images for training are selected from the LAION dataset (Schuhmann et al., 2022). We randomly select 2 million images with resolutions higher than 512 × 512. We center-crop and resize these images to 512 × 512, and pair them with the original text annotations from the LAION dataset to form image-text pairs. All images are pre-processed to compute the various conditions required for training, except for the Pose Condition. For the Pose Condition, we filter out images where no human pose was detected or key poses accounted for less than 30% of the body. We also exclude images with more than three people, as the pose detection error rate is higher in such cases.

Implementation details. In our experiments, we employed the PixelArt-α diffusion model as a representative example of the DiT model (Peebles & Xie, 2023) and StableDiffusion-2.1 (Rombach et al., 2022) as a representative example of the U-Net model. The training of the ControlNets was conducted using IDDPM (Nichol & Dhariwal, 2021), maintaining the same noise schedule as the diffusion models. All experiments were performed on four NVIDIA-RTX A6000 GPUs, employing the AdamW optimizer with a learning rate of 2×10^{-4}. The experiments were conducted with a total batch size of 64 and a total of 100,000 training steps.

Evaluation. We sample 1,000 images from the LAION Dataset for testing. Consistent with the training setting, the pose condition in the test set underwent the same image selection criteria. There are no duplicate images between the training and testing sets. To assess the controllability

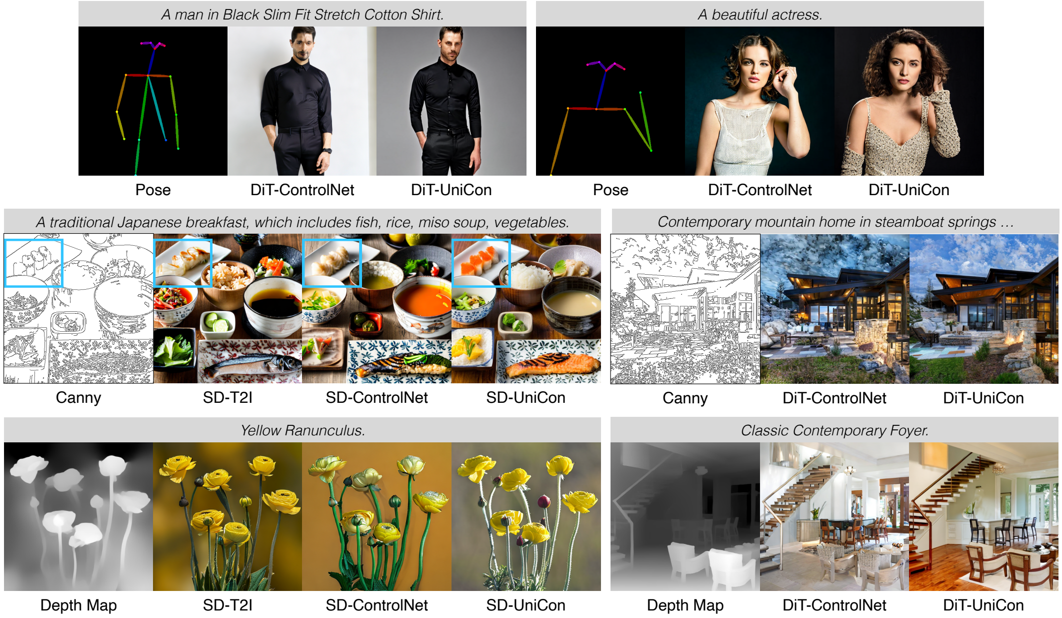

Figure 5: Comparison of different methods. We present the qualitative comparisons ControlNet (Zhang et al., 2023) and T2I (Mou et al., 2024) with both Stable Diffusion (SD) (Rombach et al., 2022) and Diffusion Transformer (DiT) (Peebles & Xie, 2023).

of different methods, we evaluate the alignment between the conditions of the generated images and the ground-truth conditions. Different metrics were chosen based on the type of condition: peak signal-to-noise ratio (PSNR) for low-level conditions; structural similarity (SSIM) (Wang et al., 2004) for canny edge conditions; mean square error (MSE) for depth conditions; and mean average precision (mAP) for object keypoint similarity in pose conditions (Zhao et al., 2024). In addition to assessing controllability, we evaluated the quality of generation using metrics such as FID (Heusel et al., 2017), Clip-IQA (Wang et al., 2023a), MAN-IQA (Yang et al., 2022), and MUSIQ (Ke et al., 2021). Furthermore, the Clip-Score (Hessel et al., 2021) was used to evaluate the consistency between generated images and their corresponding text prompts, ensuring an integrated and thorough assessment of both image quality and fidelity to conditioned inputs.

4.2 Ablation Study

The effect of copying "encoders" and copying "decoders" on diffusion control. Using ControlNet as an example, we explored the influence of different parts of diffusion models on controlled generation. The design of ControlNet involves making a trainable copy of the network's "encoder". Based on the DiT architecture, we further designed three variants. The first variant involves making a trainable copy of and controlling the "decoder" part (the latter half) of the network, as shown in Figure 3(a). The second variant controls the entire network, covering both the encoder and decoder parts. To keep the parameter number constant, we adopt a method of skipping and deleting every other block, as shown in Figure 3(b), referred to as the "Skip-Layer" design. The final variant involves making a trainable copy of the entire diffusion model, which we call the "Full" version.

We test these variants on canny and SR tasks. The results are displayed in Table 1a. First, comparing different designs focusing on the encoder and decoder, the results indicate that while focusing on the encoder leads to better image quality, focusing on the decoder enhances controllability. This is probably because the understanding and generation of images and control signals are primarily conducted in the first half of the network, whereas the precise control of generation details occurs in the latter half. Specifically, for tasks such as SR that demand precise local control, a decoder-focused design might be more suitable. Given the distinct advantages of both encoder and decoder in controlling generation, we further explored the effects of utilizing both simultaneously. The results from the Skip-Layer variant confirmed this approach, demonstrating improved generative performance

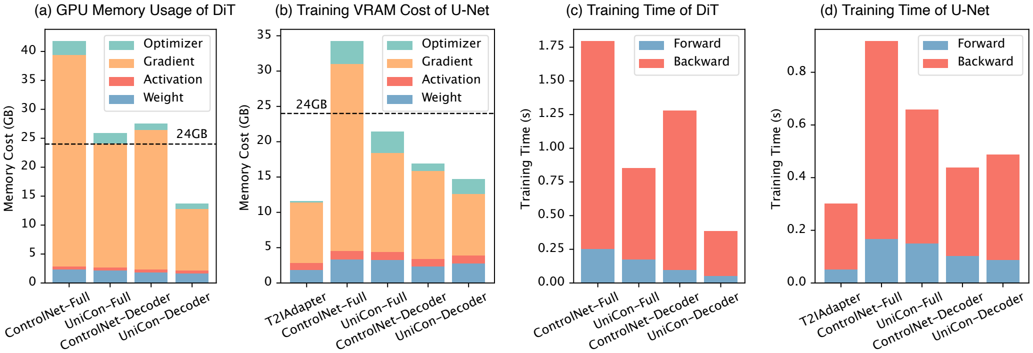

Figure 6: Comparison of training VRAM usage and training time of different adapter designs.

and controllability at the same parameter number. This proves that for DiT, distinguishing between encoder and decoder is not effective, and we should leverage the capabilities of different parts of the entire diffusion model. The Full version, building upon the Skip-Layer, further increased the parameter number, and its enhanced generative performance and controllability also affirmed the importance of adapter capacity in controlling diffusion models.

Unidirectional information flow *v.s.* changing feature directly. The method proposed in this paper differs significantly from existing approaches by introducing the concept of unidirectional information flow. Maintaining the same adapter architecture and initialization, we opted to output using adapters rather than directly changing the features of the diffusion model. We test various adapter variants mentioned above, and the results are presented in Table 1c. Our results show that employing the unidirectional information flow for output substantially enhances performance, improving controllability and generative quality in both high-level and low-level tasks, whether using the diffusion model's "decoder" part or the full model as the adapter. For the "Skip-Layer" adapter, the unidirectional information flow design did not lead to performance gains. This is intuitively due to the skip-layer design compromising the output capability of the copied diffusion model. While the Skip-Layer design enhances the effectiveness of ControlNet, it is not suitable for UniCon. This ablation study demonstrates that a simple implementation of unidirectional information flow can significantly enhance both control effectiveness and generation quality.

Training cost. A major advantage of UniCon is its computational efficiency. As gradients do not need to be computed and stored for the diffusion model, UniCon significantly reduces VRAM usage and speeds up training. We compare VRAM occupation and training speed between UniCon and ControlNet in a single-GPU setup without any acceleration libraries. All experiments maintain consistency with standard training in terms of model parameters, diffusion settings. All necessary feature maps, such as text tokens, latent condition images, and latent ground-truth images, were pre-computed. We select the same 100 training batches, each with a size of 16, and all speed tests were performed on the same NVIDIA-RTX A6000 GPU. All parameters and computations were performed in BFloat16 precision. We detail the VRAM consumption as follows: (1) Weight: VRAM used just for loading the model. (2) Activation: VRAM used for network forward propagation without gradient computation. (3) Gradient: VRAM used to store gradients. (4) Optimizer: VRAM used for updating learnable parameters of the model. We also record the time costs for network forward propagation (FP) and backward propagation (BP). FP time accounted for the time spent on the diffusion model forward step, and BP time included the total time for updating gradients and optimizer parameters. Finally, we report the peak VRAM and average time costs over 100 iterations, with results presented in Figure 6. It can be seen that UniCon significantly reduces VRAM usage compared to ControlNet, saving nearly half the storage required for gradients, which are a major component of VRAM consumption during training. In terms of training time, because it eliminates the need to compute gradients for the diffusion model, the time spent on BP is also nearly halved.

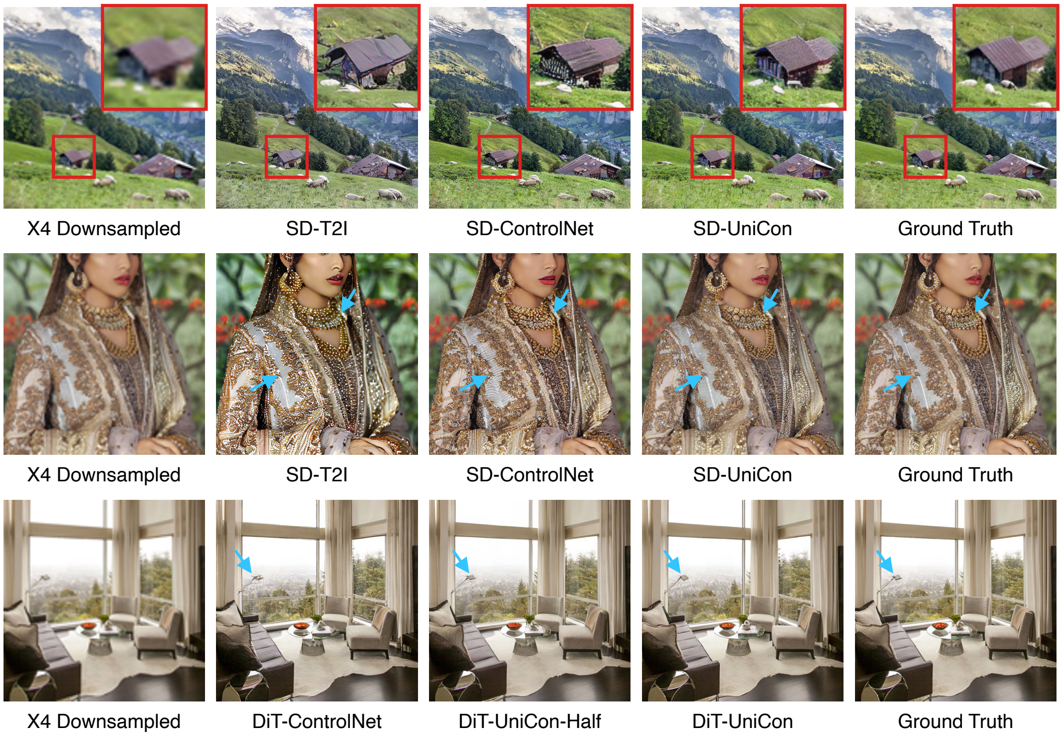

Figure 7: Comparison of different methods on conditional generation with low-level control inputs.

The choice of the connector. We explored various methods for connecting diffusion models with adapters and found that different connectors lead to different outcomes. Based on the DiT diffusion model, we test three connector designs, including ZeroMLP, which is consistent with the ControlNet (Zhang et al., 2023; Li et al., 2024), ShareAttention (Esser et al., 2024; Zhang & Agrawala, 2024), which is suited for Transformer attention layers, and ZeroFT. The results of these designs are displayed in Table 1b. The results indicate that our proposed ZeroFT connector offers superior control and generative performance for both high-level and low-level tasks.

Retaining the original diffusion model preserves the previously learned generative capabilities. During the development of UniCon, a natural question emerged: Given that the outputs are already handled by the adapter, is it necessary to retain the pre-trained diffusion model, or can we just fine-tune a part of it? We compared the UniCon structure shown in Figure 3(d) with a structure that discards part of the diffusion model as shown in Figure 3(e). Figure 4 presents the results of this comparison. The findings indicate that if the complete pre-trained diffusion model is not preserved, there is a significant decline in generative capabilities. This demonstrates that although the diffusion model in UniCon is used only for inference, the generative capabilities it has learned can still be effectively utilized by the UniCon adapter.

4.3 Comparison

We also compare UniCon with existing adapter designs. For the DiT (Peebles & Xie, 2023) diffusion models, we primarily conduct a direct comparison between UniCon and ControlNet (Zhang et al., 2023). For the SD U-Net diffusion models, we compared UniCon with both ControlNet (Zhang et al., 2023) and T2I-Adapter (Mou et al., 2024). These comparisons of controllable diffusion models were conducted across all datasets.

Table 2 shows the results. It can be seen that our proposed UniCon outperforms the ControlNet and T2I-Adapter in all tasks. In terms of controllability, UniCon excels in maintaining control signals. UniCon also outperforms existing methods in image quality metrics, especially FID scores.

Diffusion	Task	Adapter	Controllability		Generation Quality				Text Consistency
Model			Metric	Value	FID↓	Clip-IQA↑	MAN-IQA↑	MUSIQ↑	Clip-Score↑
DiT	Canny	ControlNet	SSIM↑	0.4748	51.52	0.6439	0.1861	65.24	0.7724
		UniCon	SSIM↑	**0.5458**	**46.71**	**0.6577**	**0.2029**	**66.45**	**0.7889**
	Depth	ControlNet	MSE↓	84.65	53.63	0.6469	0.1838	64.88	0.7722
		UniCon	MSE↓	**82.56**	**51.49**	**0.6514**	**0.2002**	**65.51**	**0.7785**
	Pose	ControlNet	mAP↑	0.4135	58.62	0.6332	0.1819	63.94	0.7430
		UniCon	mAP↑	**0.4627**	**57.85**	**0.6600**	**0.1929**	**65.00**	**0.7545**
	SR	ControlNet	PSNR↑	34.82	26.43	0.7147	0.2459	69.37	0.7996
		UniCon-half	PSNR↑	35.64	22.07	0.7042	0.2675	69.51	**0.8025**
		UniCon	PSNR↑	**37.34**	**20.34**	**0.7251**	**0.2831**	**69.99**	0.8022
	Deblur+ SR	ControlNet	PSNR↑	37.63	29.18	**0.7199**	0.2517	69.72	0.8004
		UniCon-half	PSNR↑	38.33	25.12	0.6998	0.2563	69.31	**0.8014**
		UniCon	PSNR↑	**41.13**	**21.29**	0.7089	**0.2701**	**69.80**	0.8012
SD U-Net	Canny	ControlNet	SSIM↑	0.4895	49.80	0.6683	0.2215	67.19	0.8168
		T2I-Adapter	SSIM↑	0.3936	52.05	**0.6783**	0.2266	**68.16**	0.8155
		UniCon	SSIM↑	**0.5570**	**47.11**	0.6704	**0.2335**	67.99	**0.8189**
	Depth	ControlNet	MSE↓	85.70	54.30	0.6828	0.2262	67.90	0.8202
		T2I-Adapter	MSE↓	87.72	55.09	**0.6906**	**0.2331**	**68.12**	0.8209
		UniCon	MSE↓	**85.00**	**53.45**	0.6807	0.2262	67.85	**0.8214**
	SR	ControlNet	PSNR↑	31.66	30.19	0.7373	0.3266	**70.94**	**0.8044**
		T2I-Adapter	PSNR↑	18.94	48.20	0.6822	0.2795	70.91	0.7812
		UniCon-half	PSNR↑	34.38	28.29	0.7387	0.3244	69.76	0.8037
		UniCon	PSNR↑	**35.69**	**22.80**	**0.7442**	**0.3271**	70.48	0.8027

Table 2: Comparisons of different controllable diffusion models. ↑ indicates the larger the better and ↓ indicates the lower the better.

It should be noted that although the T2I-Adapter method is better than UniCon in some image quality metrics, the control effect of the T2I method is not good. Combining our ablation studies and comparative experiments, we also found that the scale of the adapter impacts the final outcomes. UniCon-Half, with only half the parameters, performs notably worse than the full-parameter UniCon but still performs better than ControlNet with a comparable parameter number. Notably, even the full-parameter UniCon has a lower training computational cost than ControlNet.

Figure 5 shows some visual comparisons of high-level conditional generation tasks. As one can see that our proposed UniCon excels in generating images with superior detail structure, such as more intricate facial features, and fewer artifacts and tears. Additionally, UniCon surpasses other methods in precision control, as demonstrated in the comparison of the second row's first set. Although the sushi rolls are small in scale and complex in structure, UniCon accurately generates sushi rolls at the correct location, faithfully following the control conditions, unlike other methods that fail to strictly adhere to these conditions and their generative capabilities are inferior to UniCon. Figure 7 further illustrates UniCon's performance in low-level control generation tasks, which demand high fidelity. Our method not only maintains high-quality generation but also strictly adheres to the controls of the input images, effectively generating even the smallest structures. UniCon demonstrates better results in tasks such as image restoration and super-resolution based on diffusion models, showcasing broad application prospects. More results can be found in Appendix.

5 Conclusion

This paper presents UniCon, a novel approach tailored for controlling large-scale diffusion models. UniCon leverages unidirectional flow from the diffusion network to the adapter, simplifying the computational process by eliminating the need to compute and store gradients of the diffusion model. UniCon significantly reduces the VRAM requirements and enhances training speeds while maintaining high fidelity in generated images.

REFERENCES

Yuval Alaluf, Omer Tov, Ron Mokady, Rinon Gal, and Amit Bermano. Hyperstyle: Stylegan inversion with hypernetworks for real image editing. In *Proceedings of the IEEE/CVF conference on computer Vision and pattern recognition*, pp. 18511–18521, 2022.

Titas Anciukevičius, Zexiang Xu, Matthew Fisher, Paul Henderson, Hakan Bilen, Niloy J. Mitra, and Paul Guerrero. Renderdiffusion: Image diffusion for 3d reconstruction, inpainting and generation. In *Proceedings of the IEEE/CVF Conference on Computer Vision and Pattern Recognition (CVPR)*, pp. 12608–12618, June 2023.

Omri Avrahami, Dani Lischinski, and Ohad Fried. Blended diffusion for text-driven editing of natural images. In *Proceedings of the IEEE/CVF Conference on Computer Vision and Pattern Recognition*, pp. 18208–18218, 2022.

Omri Avrahami, Ohad Fried, and Dani Lischinski. Blended latent diffusion. *ACM Transactions on Graphics (TOG)*, 42(4):1–11, 2023.

Fan Bao, Shen Nie, Kaiwen Xue, Yue Cao, Chongxuan Li, Hang Su, and Jun Zhu. All are worth words: A vit backbone for diffusion models. In *Proceedings of the IEEE/CVF Conference on Computer Vision and Pattern Recognition*, pp. 22669–22679, 2023.

John Canny. A computational approach to edge detection. *IEEE Transactions on pattern analysis and machine intelligence*, (6):679–698, 1986.

Yu Cao, Xiangqiao Meng, PY Mok, Tong-Yee Lee, Xueting Liu, and Ping Li. Animediffusion: Anime diffusion colorization. *IEEE Transactions on Visualization and Computer Graphics*, 2024.

Z. Cao, G. Hidalgo Martinez, T. Simon, S. Wei, and Y. A. Sheikh. Openpose: Realtime multi-person 2d pose estimation using part affinity fields. *IEEE Transactions on Pattern Analysis and Machine Intelligence*, 2019.

Junsong Chen, Jincheng Yu, Chongjian Ge, Lewei Yao, Enze Xie, Yue Wu, Zhongdao Wang, James Kwok, Ping Luo, Huchuan Lu, and Zhenguo Li. Pixart-α: Fast training of diffusion transformer for photorealistic text-to-image synthesis, 2023.

Junsong Chen, Chongjian Ge, Enze Xie, Yue Wu, Lewei Yao, Xiaozhe Ren, Zhongdao Wang, Ping Luo, Huchuan Lu, and Zhenguo Li. Pixart-σ: Weak-to-strong training of diffusion transformer for 4k text-to-image generation, 2024a.

Junsong Chen, Yue Wu, Simian Luo, Enze Xie, Sayak Paul, Ping Luo, Hang Zhao, and Zhenguo Li. Pixart-δ: Fast and controllable image generation with latent consistency models, 2024b.

Max Daniels, Tyler Maunu, and Paul Hand. Score-based generative neural networks for large-scale optimal transport. *Advances in neural information processing systems*, 34:12955–12965, 2021.

Johann-Friedrich Feiden Denis Zavadski and Carsten Rother. Controlnet-xs: Designing an efficient and effective architecture for controlling text-to-image diffusion models. 2023.

Tan M Dinh, Anh Tuan Tran, Rang Nguyen, and Binh-Son Hua. Hyperinverter: Improving stylegan inversion via hypernetwork. In *Proceedings of the IEEE/CVF Conference on Computer Vision and Pattern Recognition*, pp. 11389–11398, 2022.

Patrick Esser, Sumith Kulal, Andreas Blattmann, Rahim Entezari, Jonas Müller, Harry Saini, Yam Levi, Dominik Lorenz, Axel Sauer, Frederic Boesel, et al. Scaling rectified flow transformers for high-resolution image synthesis. *arXiv preprint arXiv:2403.03206*, 2024.

Ligong Han, Yinxiao Li, Han Zhang, Peyman Milanfar, Dimitris Metaxas, and Feng Yang. Svdiff: Compact parameter space for diffusion fine-tuning. In *Proceedings of the IEEE/CVF International Conference on Computer Vision*, pp. 7323–7334, 2023.

Jack Hessel, Ari Holtzman, Maxwell Forbes, Ronan Le Bras, and Yejin Choi. Clipscore: A reference-free evaluation metric for image captioning. *arXiv preprint arXiv:2104.08718*, 2021.

Martin Heusel, Hubert Ramsauer, Thomas Unterthiner, Bernhard Nessler, and Sepp Hochreiter. Gans trained by a two time-scale update rule converge to a local nash equilibrium. *Advances in neural information processing systems*, 30, 2017.

Jonathan Ho and Tim Salimans. Classifier-free diffusion guidance. *arXiv preprint arXiv:2207.12598*, 2022.

Jonathan Ho, Ajay Jain, and Pieter Abbeel. Denoising diffusion probabilistic models. *Advances in neural information processing systems*, 33:6840–6851, 2020.

Neil Houlsby, Andrei Giurgiu, Stanislaw Jastrzebski, Bruna Morrone, Quentin De Laroussilhe, Andrea Gesmundo, Mona Attariyan, and Sylvain Gelly. Parameter-efficient transfer learning for nlp. In *International conference on machine learning*, pp. 2790–2799. PMLR, 2019.

Edward J Hu, Yelong Shen, Phillip Wallis, Zeyuan Allen-Zhu, Yuanzhi Li, Shean Wang, Lu Wang, and Weizhu Chen. Lora: Low-rank adaptation of large language models. *arXiv preprint arXiv:2106.09685*, 2021.

Yuming Jiang, Shuai Yang, Haonan Qiu, Wayne Wu, Chen Change Loy, and Ziwei Liu. Text2human: Text-driven controllable human image generation. *ACM Transactions on Graphics (TOG)*, 41(4):1–11, 2022.

Xuan Ju, Xian Liu, Xintao Wang, Yuxuan Bian, Ying Shan, and Qiang Xu. Brushnet: A plug-and-play image inpainting model with decomposed dual-branch diffusion. *arXiv preprint arXiv:2403.06976*, 2024.

Bahjat Kawar, Michael Elad, Stefano Ermon, and Jiaming Song. Denoising diffusion restoration models. *Advances in Neural Information Processing Systems*, 35:23593–23606, 2022.

Junjie Ke, Qifei Wang, Yilin Wang, Peyman Milanfar, and Feng Yang. Musiq: Multi-scale image quality transformer. In *Proceedings of the IEEE/CVF international conference on computer vision*, pp. 5148–5157, 2021.

Xiangtao Kong, Xina Liu, Jinjin Gu, Yu Qiao, and Chao Dong. Reflash dropout in image super-resolution. In *Proceedings of the IEEE/CVF Conference on Computer Vision and Pattern Recognition*, pp. 6002–6012, 2022.

Bo Li, Kaitao Xue, Bin Liu, and Yu-Kun Lai. Bbdm: Image-to-image translation with brownian bridge diffusion models. In *Proceedings of the IEEE/CVF conference on computer vision and pattern Recognition*, pp. 1952–1961, 2023a.

Ming Li, Taojiannan Yang, Huafeng Kuang, Jie Wu, Zhaoning Wang, Xuefeng Xiao, and Chen Chen. Controlnet++: Improving conditional controls with efficient consistency feedback. *arXiv preprint arXiv:2404.07987*, 2024.

Yanghao Li, Hanzi Mao, Ross Girshick, and Kaiming He. Exploring plain vision transformer backbones for object detection. In *European Conference on Computer Vision*, pp. 280–296. Springer, 2022.

Yuheng Li, Haotian Liu, Qingyang Wu, Fangzhou Mu, Jianwei Yang, Jianfeng Gao, Chunyuan Li, and Yong Jae Lee. Gligen: Open-set grounded text-to-image generation. In *Proceedings of the IEEE/CVF Conference on Computer Vision and Pattern Recognition*, pp. 22511–22521, 2023b.

Shanchuan Lin, Anran Wang, and Xiao Yang. Sdxl-lightning: Progressive adversarial diffusion distillation. *arXiv preprint arXiv:2402.13929*, 2024.

Xinqi Lin, Jingwen He, Ziyan Chen, Zhaoyang Lyu, Ben Fei, Bo Dai, Wanli Ouyang, Yu Qiao, and Chao Dong. Diffbir: Towards blind image restoration with generative diffusion prior. *arXiv preprint arXiv:2308.15070*, 2023.

Andreas Lugmayr, Martin Danelljan, Andres Romero, Fisher Yu, Radu Timofte, and Luc Van Gool. Repaint: Inpainting using denoising diffusion probabilistic models. In *Proceedings of the IEEE/CVF conference on computer vision and pattern recognition*, pp. 11461–11471, 2022.

Simian Luo, Yiqin Tan, Suraj Patil, Daniel Gu, Patrick von Platen, Apolinário Passos, Longbo Huang, Jian Li, and Hang Zhao. Lcm-lora: A universal stable-diffusion acceleration module. *arXiv preprint arXiv:2311.05556*, 2023.

Arun Mallya and Svetlana Lazebnik. Packnet: Adding multiple tasks to a single network by iterative pruning. In *Proceedings of the IEEE conference on Computer Vision and Pattern Recognition*, pp. 7765–7773, 2018.

Arun Mallya, Dillon Davis, and Svetlana Lazebnik. Piggyback: Adapting a single network to multiple tasks by learning to mask weights. In *Proceedings of the European conference on computer vision (ECCV)*, pp. 67–82, 2018.

Chenlin Meng, Yutong He, Yang Song, Jiaming Song, Jiajun Wu, Jun-Yan Zhu, and Stefano Ermon. Sdedit: Guided image synthesis and editing with stochastic differential equations. *arXiv preprint arXiv:2108.01073*, 2021.

Gautam Mittal, Jesse Engel, Curtis Hawthorne, and Ian Simon. Symbolic music generation with diffusion models. *arXiv preprint arXiv:2103.16091*, 2021.

Sicheng Mo, Fangzhou Mu, Kuan Heng Lin, Yanli Liu, Bochen Guan, Yin Li, and Bolei Zhou. Freecontrol: Training-free spatial control of any text-to-image diffusion model with any condition. *arXiv preprint arXiv:2312.07536*, 2023.

Chong Mou, Xintao Wang, Liangbin Xie, Yanze Wu, Jian Zhang, Zhongang Qi, and Ying Shan. T2i-adapter: Learning adapters to dig out more controllable ability for text-to-image diffusion models. In *Proceedings of the AAAI Conference on Artificial Intelligence*, volume 38, pp. 4296–4304, 2024.

Alex Nichol, Prafulla Dhariwal, Aditya Ramesh, Pranav Shyam, Pamela Mishkin, Bob McGrew, Ilya Sutskever, and Mark Chen. Glide: Towards photorealistic image generation and editing with text-guided diffusion models. *arXiv preprint arXiv:2112.10741*, 2021.

Alexander Quinn Nichol and Prafulla Dhariwal. Improved denoising diffusion probabilistic models. In *International conference on machine learning*, pp. 8162–8171. PMLR, 2021.

William Peebles and Saining Xie. Scalable diffusion models with transformers. In *Proceedings of the IEEE/CVF International Conference on Computer Vision*, pp. 4195–4205, 2023.

Bohao Peng, Jian Wang, Yuechen Zhang, Wenbo Li, Ming-Chang Yang, and Jiaya Jia. Controlnext: Powerful and efficient control for image and video generation. *arXiv preprint arXiv:2408.06070*, 2024.

Pablo Pernias, Dominic Rampas, Mats L. Richter, Christopher J. Pal, and Marc Aubreville. Wuerstchen: An efficient architecture for large-scale text-to-image diffusion models, 2023.

Dustin Podell, Zion English, Kyle Lacey, Andreas Blattmann, Tim Dockhorn, Jonas Müller, Joe Penna, and Robin Rombach. Sdxl: Improving latent diffusion models for high-resolution image synthesis. *arXiv preprint arXiv:2307.01952*, 2023.

René Ranftl, Alexey Bochkovskiy, and Vladlen Koltun. Vision transformers for dense prediction. In *Proceedings of the IEEE/CVF international conference on computer vision*, pp. 12179–12188, 2021.

Robin Rombach, Andreas Blattmann, Dominik Lorenz, Patrick Esser, and Björn Ommer. High-resolution image synthesis with latent diffusion models. In *Proceedings of the IEEE/CVF conference on computer vision and pattern recognition*, pp. 10684–10695, 2022.

Amir Rosenfeld and John K Tsotsos. Incremental learning through deep adaptation. *IEEE transactions on pattern analysis and machine intelligence*, 42(3):651–663, 2018.

Chitwan Saharia, William Chan, Huiwen Chang, Chris Lee, Jonathan Ho, Tim Salimans, David Fleet, and Mohammad Norouzi. Palette: Image-to-image diffusion models. In *ACM SIGGRAPH 2022 conference proceedings*, pp. 1–10, 2022a.

Chitwan Saharia, William Chan, Saurabh Saxena, Lala Li, Jay Whang, Emily L Denton, Kamyar Ghasemipour, Raphael Gontijo Lopes, Burcu Karagol Ayan, Tim Salimans, et al. Photorealistic text-to-image diffusion models with deep language understanding. *Advances in neural information processing systems*, 35:36479–36494, 2022b.

Chitwan Saharia, Jonathan Ho, William Chan, Tim Salimans, David J Fleet, and Mohammad Norouzi. Image super-resolution via iterative refinement. *IEEE transactions on pattern analysis and machine intelligence*, 45 (4):4713–4726, 2022c.

Axel Sauer, Dominik Lorenz, Andreas Blattmann, and Robin Rombach. Adversarial diffusion distillation. *arXiv preprint arXiv:2311.17042*, 2023.

Christoph Schuhmann, Romain Beaumont, Richard Vencu, Cade Gordon, Ross Wightman, Mehdi Cherti, Theo Coombes, Aarush Katta, Clayton Mullis, Mitchell Wortsman, et al. Laion-5b: An open large-scale dataset for training next generation image-text models. *Advances in Neural Information Processing Systems*, 35: 25278–25294, 2022.

Joan Serra, Didac Suris, Marius Miron, and Alexandros Karatzoglou. Overcoming catastrophic forgetting with hard attention to the task. In *International conference on machine learning*, pp. 4548–4557. PMLR, 2018.

Jascha Sohl-Dickstein, Eric Weiss, Niru Maheswaranathan, and Surya Ganguli. Deep unsupervised learning using nonequilibrium thermodynamics. In *International conference on machine learning*, pp. 2256–2265. PMLR, 2015.

Jiaming Song, Chenlin Meng, and Stefano Ermon. Denoising diffusion implicit models. *arXiv preprint arXiv:2010.02502*, 2020.

Asa Cooper Stickland and Iain Murray. Bert and pals: Projected attention layers for efficient adaptation in multi-task learning. In *International Conference on Machine Learning*, pp. 5986–5995. PMLR, 2019.

Jianyi Wang, Kelvin CK Chan, and Chen Change Loy. Exploring clip for assessing the look and feel of images. In *Proceedings of the AAAI Conference on Artificial Intelligence*, volume 37, pp. 2555–2563, 2023a.

Jianyi Wang, Zongsheng Yue, Shangchen Zhou, Kelvin CK Chan, and Chen Change Loy. Exploiting diffusion prior for real-world image super-resolution. *arXiv preprint arXiv:2305.07015*, 2023b.

Xintao Wang, Ke Yu, Shixiang Wu, Jinjin Gu, Yihao Liu, Chao Dong, Yu Qiao, and Chen Change Loy. Esrgan: Enhanced super-resolution generative adversarial networks. In *Proceedings of the European conference on computer vision (ECCV) workshops*, pp. 0–0, 2018.

Zhou Wang, Alan C Bovik, Hamid R Sheikh, and Eero P Simoncelli. Image quality assessment: from error visibility to structural similarity. *IEEE transactions on image processing*, 13(4):600–612, 2004.

Enze Xie, Lewei Yao, Han Shi, Zhili Liu, Daquan Zhou, Zhaoqiang Liu, Jiawei Li, and Zhenguo Li. Difffit: Unlocking transferability of large diffusion models via simple parameter-efficient fine-tuning. In *Proceedings of the IEEE/CVF International Conference on Computer Vision*, pp. 4230–4239, 2023.

Sidi Yang, Tianhe Wu, Shuwei Shi, Shanshan Lao, Yuan Gong, Mingdeng Cao, Jiahao Wang, and Yujiu Yang. Maniqa: Multi-dimension attention network for no-reference image quality assessment. In *Proceedings of the IEEE/CVF Conference on Computer Vision and Pattern Recognition*, pp. 1191–1200, 2022.

Tao Yang, Peiran Ren, Xuansong Xie, and Lei Zhang. Pixel-aware stable diffusion for realistic image super-resolution and personalized stylization. *arXiv preprint arXiv:2308.14469*, 2023.

Fanghua Yu, Jinjin Gu, Zheyuan Li, Jinfan Hu, Xiangtao Kong, Xintao Wang, Jingwen He, Yu Qiao, and Chao Dong. Scaling up to excellence: Practicing model scaling for photo-realistic image restoration in the wild. *arXiv preprint arXiv:2401.13627*, 2024.

Denis Zavadski, Johann-Friedrich Feiden, and Carsten Rother. Controlnet-xs: Designing an efficient and effective architecture for controlling text-to-image diffusion models. *arXiv preprint arXiv:2312.06573*, 2023.

Lvmin Zhang and Maneesh Agrawala. Transparent image layer diffusion using latent transparency. *arXiv preprint arXiv:2402.17113*, 2024.

Lvmin Zhang, Anyi Rao, and Maneesh Agrawala. Adding conditional control to text-to-image diffusion models. In *Proceedings of the IEEE/CVF International Conference on Computer Vision*, pp. 3836–3847, 2023.

Min Zhao, Fan Bao, Chongxuan Li, and Jun Zhu. Egsde: Unpaired image-to-image translation via energy-guided stochastic differential equations. *Advances in Neural Information Processing Systems*, 35:3609–3623, 2022.

Shihao Zhao, Dongdong Chen, Yen-Chun Chen, Jianmin Bao, Shaozhe Hao, Lu Yuan, and Kwan-Yee K Wong. Uni-controlnet: All-in-one control to text-to-image diffusion models. *Advances in Neural Information Processing Systems*, 36, 2024.

A Broader Impact

Controlled generation technology, as a pivotal innovation in the field of diffusion models, exerts a significant impact across multiple sectors of society. In the creative industries, it enables artists and designers to realize complex visions with unprecedented precision and flexibility, fostering innovation in digital art, design, and multimedia content creation. In commercial applications, controlled generation technology enhances marketing strategies by offering more targeted and dynamic advertising visuals, effectively engaging consumers. Additionally, its influence extends to education and training, where it can revolutionize teaching methods and materials, especially in visually-dependent disciplines, by generating customized educational content and simulations.

Although our system enables artists, designers, and content creators to realize their creative visions through precise control, it is crucial to recognize the potential negative societal impacts that could arise from misuse or abuse, similar to other AI models for image generation and editing. To address these issues, responsible deployment practices, ethical standards, and including special markers in generated images to increase transparency are essential steps in achieving responsible use.

B Limitations

UniCon's training process eliminates the need for the gradient of the base generative model, significantly reducing computational overhead. However, UniCon does not decrease the network's parameter count, resulting in limited speed improvement during sampling compared to DiT-ControlNet.

C More Details

Comparison Models. In our experiment with the stable diffusion v2.1 (SD), we employ the official versions of the ControlNet (Zhang et al., 2023) and T2IAdapter (Mou et al., 2024) models without any modifications. Since ControlNet is originally designed for U-Net, there is no official version compatible with the DiT transformer-base diffusion model. Therefore, the DiT-ControlNet variant used in our study is a reproduction by PixArt-α (Chen et al., 2023). Following the design principles of ControlNet, the initial halves of the DiT blocks are copied and trained as the controller. The primary difference from the U-Net-based ControlNet is the lack of skip connections in DiT-ControlNet. This makes DiT-ControlNet unable to detach the gradient of the "Encoder" part of the base model, significantly increasing peak VRAM usage.

Sampling scheme. We employ a second-order DPM solver sampler to generate images, with a sampling step of 24. In our PixArt (Chen et al., 2023) experiment, we incorporated null tokens as negative prompts and applied a CFG (Ho & Salimans, 2022) scale of 4.5. Conversely, in the SD v2.1 experiment, the negative prompt included terms such as *"blurring, dirty, messy, worst quality, low quality, frames, watermark, signature, jpeg artifacts, deformed, low-res, over-smooth"*, and we used a CFG scale of 7.5.

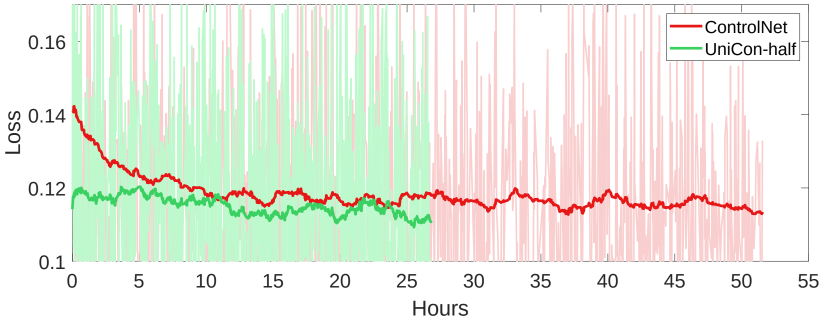

Figure 8: Comparison of training curves between ControlNet and UniCon-half for 100K iterations under Canny edge condition. Notice that ControlNet and UniCon have similar values at the start of training, but show differences after smoothing due to UniCon's faster convergence.

Task	Training Steps	Controllability		Generation Quality				Text Consistency
		Metric	Value	FID↓	Clip-IQA↑	MAN-IQA↑	MUSIQ↑	Clip-Score↑
Canny	50K	SSIM↑	0.2974	70.40	0.4326	0.1167	50.96	0.7623
	100K	SSIM↑	0.5458	46.71	0.6577	0.2029	66.45	0.7889
	200K	SSIM↑	0.5400	46.49	0.6529	0.2079	**66.78**	0.7898
	400K	SSIM↑	**0.5507**	**46.13**	**0.6633**	**0.2082**	66.50	**0.7933**
LQ	50K	PSNR↑	36.48	22.86	0.6996	0.2401	68.43	0.7909
	100K	PSNR↑	37.34	20.34	0.7251	0.2831	69.99	**0.8022**
	200K	PSNR↑	**37.40**	20.07	0.7172	**0.2846**	69.42	0.8014
	400K	PSNR↑	37.35	**19.94**	**0.7291**	0.2819	**69.97**	0.8009

Table 3: Comparisons of different training steps for DiT-UniCon-Full. ↑ indicates the larger the better and ↓ indicates the lower the better. **Bold** represents the best performance.

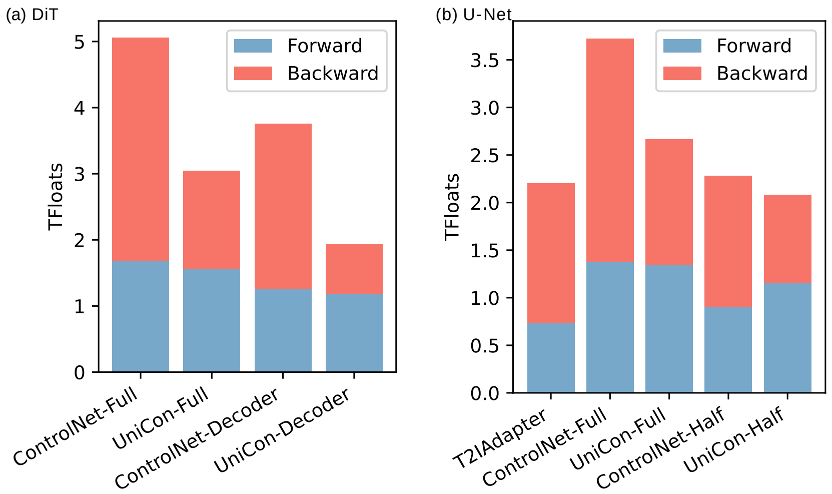

Figure 9: Comparison of (a) DiT and (b) U-Net forward and backward propagating TFloats with different adapters.

Metric calculations. We computed PSNR, SSIM, LPIPS, CLIP-IQA, MANIQA, and MUSIQ using the pyiqa library[1], with PSNR specifically calculated on the Y channel. FID scores were determined via the clean-FID[2]. Additionally, MSE was calculated in the RGB domain, with values ranging from 0 to 256. We adopt the mean average precision (mAP) based on object keypoint similarity (OKS) from (Cao et al., 2019; Zhao et al., 2024) as the metric for the pose condition.

Convergence tendency. To highlight UniCon's training advantages, we compared its convergence trends with ControlNet. As shown in Figure 8, UniCon retains ControlNet's fast convergence. Despite reversing the direction of information flow, UniCon ensures effective initialization by using a zero-initialized Connector Block and copying parameters from the pre-trained base model.

Training Steps. We evaluated the performance of UniCon across varying training steps to identify the optimal step size. As presented in Table 3, UniCon fails to converge at 50K steps for both LQ and Canny tasks. Performance improves substantially from 50K to 100K steps, while further increases beyond 100K yield only marginal gains. Hence, 100K steps is determined to be the most cost-effective training step size.

Computational evaluation. As shown in Figure 9, we further analyzed the computational cost of each adaptor during forward and backward propagation. With the same number of learnable parameters, UniCon's total computational cost is lower than ControlNet's. In the UNet-Half setting, UniCon's FP TFloats are slightly higher because it copies the Decoder, which has more parameters

[1] https://github.com/chaofengc/IQA-PyTorch
[2] https://github.com/GaParmar/clean-fid

Task	Adapter	Controllability			Generation Quality			Text Consistency
		Metric	Value	FID↓	Clip-IQA↑	MAN-IQA↑	MUSIQ↑	Clip-Score↑
Canny	ControlNet	SSIM↑	0.4895	49.80	0.6683	0.2215	67.19	0.8168
	UniControlNet	SSIM↑	0.4996	49.95	0.6749	**0.2348**	67.95	0.8152
	GLIGEN	SSIM↑	0.4447	55.42	**0.6802**	0.2280	67.91	0.7901
	T2I-Adapter	SSIM↑	0.3936	52.05	0.6783	0.2266	**68.16**	0.8155
	ControlNeXt	SSIM↑	0.4568	53.03	0.6616	0.2153	66.68	0.8141
	UniCon	SSIM↑	**0.5570**	**47.11**	0.6704	0.2335	67.99	**0.8189**
Depth	ControlNet	MSE↓	85.70	54.30	0.6828	0.2262	67.90	0.8202
	UniControlNet	MSE↓	85.89	54.49	0.6846	0.2302	67.89	**0.8217**
	GLIGEN	MSE↓	87.65	58.25	0.6851	0.2234	**68.41**	0.7964
	T2I-Adapter	MSE↓	87.74	55.09	**0.6906**	**0.2331**	68.12	0.8209
	ControlNeXt	MSE↓	86.81	55.71	0.6799	0.2291	68.00	0.8198
	UniCon	MSE↓	**85.00**	**53.45**	0.6807	0.2262	67.85	0.8214

Table 4: Comparisons of different adapters for SD-UNet. ↑ indicates the larger the better and ↓ indicates the lower the better. **Bold** represents the best performance.

Adaptor	Base Model	PSNR↑	LPIPS↓	MUSIQ↑	CLIP-Score↑	FID↓
StableSR	SD2.1	35.39	0.0839	69.57	0.7786	37.85
DiffBIR	SD2.1	34.81	0.0940	69.76	0.7844	32.85
PASD	SD2.1	36.17	0.0552	69.62	0.7925	25.61
UniCon	SD2.1	35.69	0.0530	**70.48**	**0.8027**	22.80
UniCon	PixArt-α	**37.34**	**0.0453**	69.99	0.8022	**20.34**

Table 5: Results of different diffusion-based image restoration models. ↑ indicates the larger the better and ↓ indicates the lower the better. **Bold** represents the best performance.

than ControlNet's copied Encoder. While T2I-Adaptor has the lowest FP TFloats, its control capability is significantly weaker than UniCon's, and its performance degrades noticeably in low-level tasks, as shown in Table 2.

D Pseudo Codes

Training Cost Experiments. In Algorithm 1, we present a pseudo code to evaluate the single-round training cost. The sampling methods for training noise and timestep remain consistent with those used during training. We subsequently report the peak memory usage and average time based on one hundred rounds of training cost evaluation.

Core Difference between ControlNet and UniCon. Algorithm 2 and Algorithm 3 illustrate the pseudo codes for the forward passes of ControlNet and UniCon, respectively. Unlike ControlNet, UniCon avoids storing the base model's gradients during forward propagation and truncates all gradient connections from the base model to the controller. Consequently, the base model gradients are not utilized during backpropagation. These modifications significantly reduce UniCon's memory overhead and training time compared to ControlNet.

E More Comparison Results

More Adapters on Highlevel Tasks. To comprehensively compare UniCon's performance, we evaluated it against other high-level control methods on the UNet model, including UniControlNet (Zhao et al., 2024), GLIGEN (Li et al., 2023b), and ControNeXt (Peng et al., 2024). As shown in Table 4, UniCon achieved the best controllability and FID scores on both canny and depth tasks. NR metrics confirm that UniCon maintains strong control capabilities without notably compromising image quality.

More Adapters on Lowlevel Tasks. Considering that several diffusion-based methods have been applied to low-level tasks, we compared UniCon with related approaches in image restoration (Wang et al., 2023b; Lin et al., 2023; Yang et al., 2023). As shown in Table 5, with SD2.1 as the base

Adapter	Condition Consistency			Image Quality			Text Consistency	Diversity
	PSNR↑	SSIM↑	LPIPS↓	Clip-IQA↑	MAN-IQA↑	MUSIQ↑	Clip-Score↑	FID↓
ControlNet	34.82	0.9352	0.0650	0.7147	0.2459	69.37	0.7996	26.43
ControlNeXt	34.31	0.9329	0.0679	0.7171	0.2534	69.36	0.7997	26.28
UniCon-Half	35.64	**0.9512**	0.0475	0.7042	0.2675	69.51	**0.8025**	22.07
UniCon-Half†	**36.41**	**0.9512**	**0.0462**	**0.7189**	**0.2782**	**69.66**	0.8008	**21.34**

Table 6: Comparisons of different adapters for PixArt-α on $\times 4$ Super-Resolution task. † represents the use of the pre-trained ControlNeXt model as the base model. ↑ indicates the larger the better and ↓ indicates the lower the better. **Bold** represents the best performance.

model, UniCon achieves the highest image quality, with fidelity significantly surpassing StableSR and DiffBIR, and comparable to PASD. Furthermore, using PixArt-α as the base model, UniCon's fidelity improves significantly.

Discussion of ControlNeXt. Since ControlNeXt introduces only a small number of additional parameters during training (Peng et al., 2024), it offers a significant advantage in inference speed compared to other ControlNet variants. However, as shown in Table 6, ControlNeXt's control capabilities are slightly below ControlNet and significantly behind UniCon. While UniCon requires longer inference time, it delivers better performance in scenarios with stricter consistency requirements. Additionally, we found that UniCon and ControlNeXt offer complementary benefits. Using ControlNeXt as UniCon's pre-trained model significantly boosts UniCon's performance, achieving much higher fidelity and quality than ControlNet with the same number of parameters. This two-stage training process can be viewed as a course-to-fine approach with high efficiency.

Visual Comparison. Due to space limitations, we provide more visual comparison results in Figure 14, Figure 15 and Figure 16. Massive visual comparisons prove our method not only maintains high-quality generation but also strictly adheres to the controls of the input images.

F Full Ablation Study Results

Due to space limitations in the main text, we only present some results in the main text. We present the complete ablation experimental results in Table 7, Figure 10, Figure 11, Figure 12 and Figure 13.

The Effect of Copying "Encoders" and "Decoders" on Diffusion Control. Visual comparisons of different adapter structures in Figure 10 reveal that the "Encoders" model exhibits insufficient controllability. In the canny task, this inadequacy manifests as the addition of objects misaligned with the canny lines, such as the giraffe's neck in Figure 10(a). In the SR task, it results in color shifts and artifacts, such as the overall darkness and the sky with messy spots in Figure 10(b). Conversely, while copying "Decoders" improves controllability, it compromises the quality of the generated images, as evidenced by the coloring errors on the face in Figure 10(a) and the messy textures on vegetables and human faces in Figure 10(b). This aligns with the conclusion that focusing on encoders leads to better generation effects, whereas focusing on decoders enhances controllability. As shown in Table 7, the "Skip-Layer" type achieves the highest controllability and image quality among the three copying schemes with the same parameter count. The "Full" copying structure achieves higher metrics and better visual effects by adding parameters on top of the "Skip-Layer" structure, as demonstrated in Figure 10(a), where the "Full" type maintains facial features intact from multiple angles.

Unidirectional Information Flow vs. Changing Features Directly. As indicated in Table 7, using adapters as outputs under the "Skip-Layer" structure negatively impacts the Canny task and causes collapses in the SR task. This likely results from error accumulation in the adapters during initialization with the "Skip-Layer" copying scheme. These errors are less influential when the base diffusion model is used as the output but affect training stability when adapters directly output. Beyond the "Skip-Layer" type, unidirectional information flow steadily improves the model's controllability. In the canny task, unidirectional information flow produces results more consistent with the conditioned lines, as seen in Figure 11(a): the "Full" case 1 curtains and the "Decoder" case 1 water surface. In the SR task, it enhances fidelity, as exemplified by the Chinese string in Figure 11(b). In conclusion, Figure 11 shows that unidirectional information flow significantly reduces training overhead while maintaining overall image quality without degradation.

The Choice of Connector. As demonstrated in Table 7, using ZeroFT as the connector in both the Canny and SR tasks maintains the highest controllability and image quality metrics. Employing ZeroFT enables the network to effectively manage relationships between objects in complex scenes. For instance, with ZeroFT, the network can generate a more natural half-length photo of the woman in Figure 12(a) and accurately process the margin between the hollow chandelier and wall in Figure 12(b).

The Influence of Cross-Attention Blocks in Adapters. Previous work, such as BrushNet (Ju et al., 2024), has discussed that removing cross-attention blocks connected to the text prompt in the Adapter module can enhance the fidelity of ControlNet. We investigated whether this approach would also be effective for UniCon. Therefore, we tested the impact of removing cross-attention blocks in the canny and SR tasks in our complete ablation study. As shown in Table 7, removing cross-attention blocks decreases all metrics in the canny task but improves them in the SR task. Visually, dropping cross-attention causes incorrect color matching in the canny task, as seen in Figure 13(a). However, in the SR task, it prevents the generation of cluttered high-frequency textures, as illustrated in Figure 13(b). We speculate that this is because the SR condition already provides sufficient information, making the text prompt less critical, while excessive text guidance can cause CFG to produce messy high-frequency textures. In the canny task, the network relies more on the text prompt to supplement the information that the condition alone cannot provide. Consequently, we removed the cross-attention module in adapters for the SR and Blur+SR tasks.

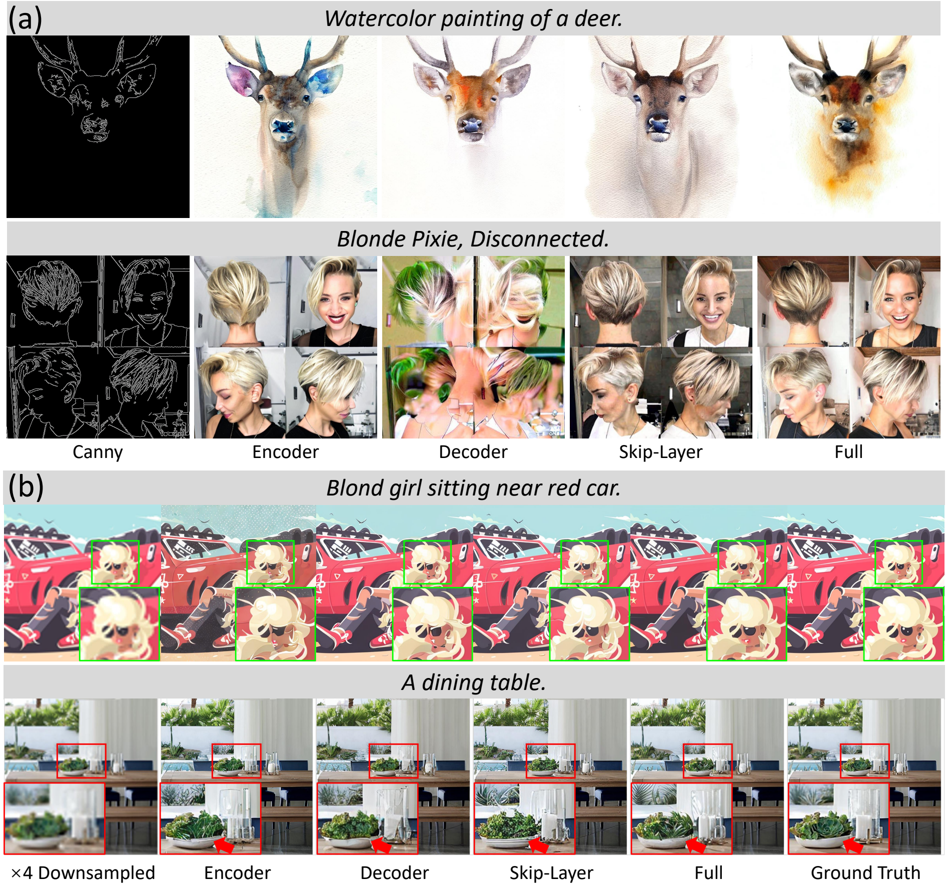

Figure 10: Comparison of different variants of UniCon on conditional generation with (a) Canny and (b) downsampled images.

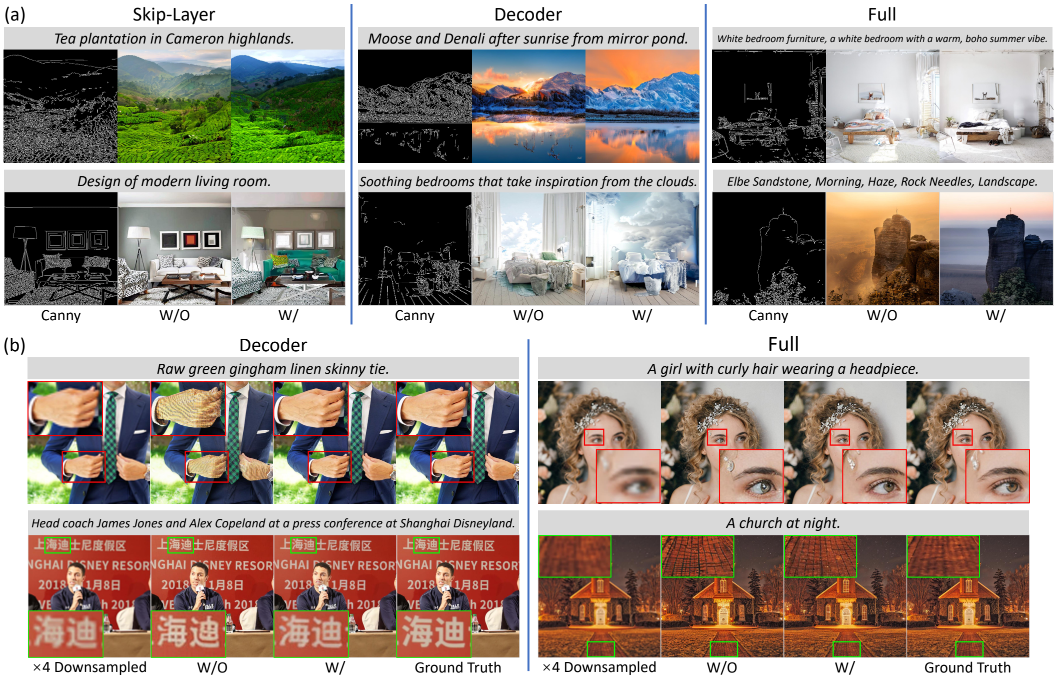
(a)
Skip-Layer
Tea plantation in Cameron highlands.
Design of modern living room.
Decoder
Moose and Denali after sunrise from mirror pond.
Soothing bedrooms that take inspiration from the clouds.
Full
White bedroom furniture, a white bedroom with a warm, boho summer vibe.
Elbe Sandstone, Morning, Haze, Rock Needles, Landscape.
Canny
W/O
W/
(b)
Decoder
Raw green gingham linen skinny tie.
Head coach James Jones and Alex Copeland at a press conference at Shanghai Disneyland.
Full
A girl with curly hair wearing a headpiece.
A church at night.
×4 Downsampled
W/O
W/
Ground Truth

Figure 11: Comparison of different variants of UniCon with or without unidirectional flow on conditional generation with (a) Canny and (b) downsampled images.

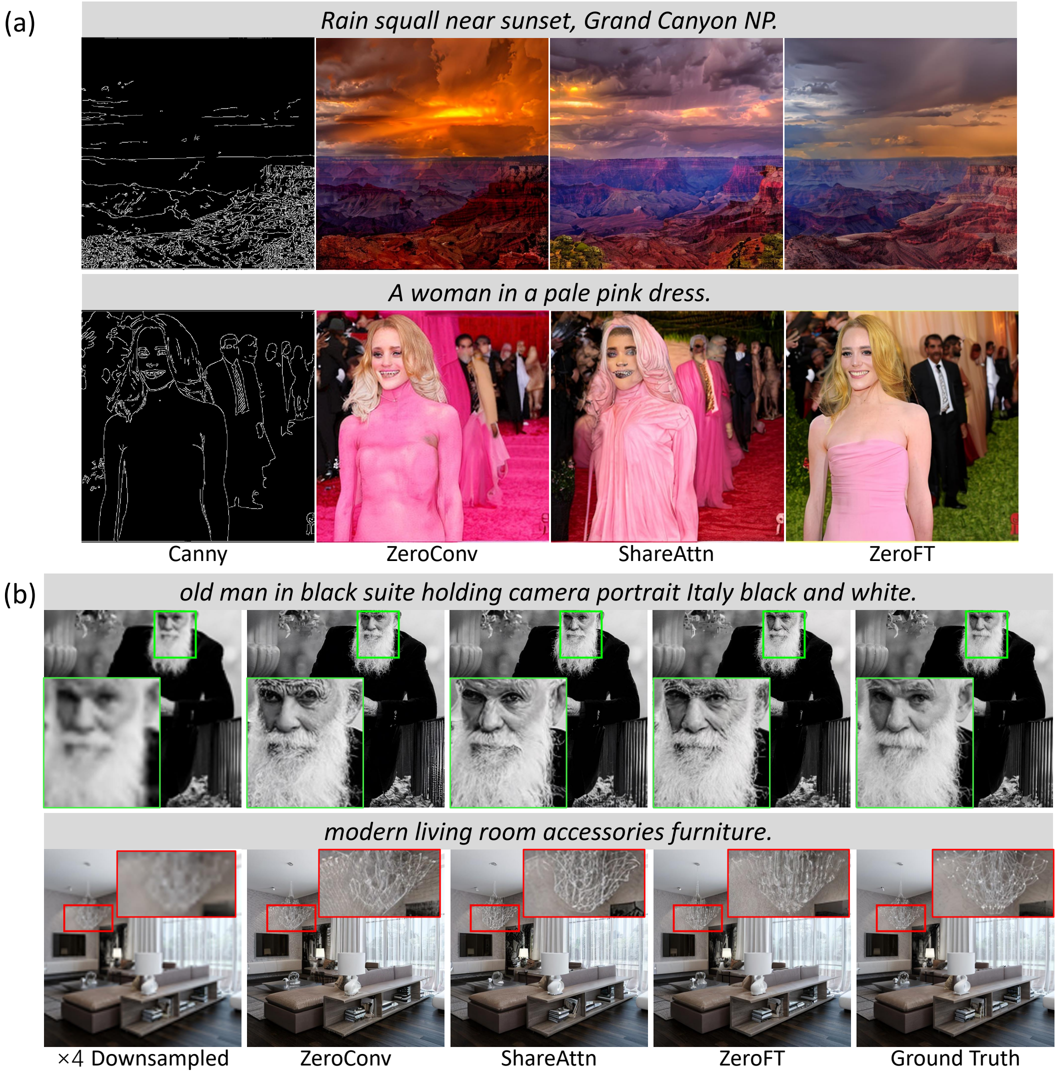
(a)
Rain squall near sunset, Grand Canyon NP.
A woman in a pale pink dress.
Canny
ZeroConv
ShareAttn
ZeroFT
(b)
old man in black suite holding camera portrait Italy black and white.
modern living room accessories furniture.
×4 Downsampled
ZeroConv
ShareAttn
ZeroFT
Ground Truth

Figure 12: Comparison of UniCon using different connectors on conditional generation with (a) Canny and (b) downsampled images.

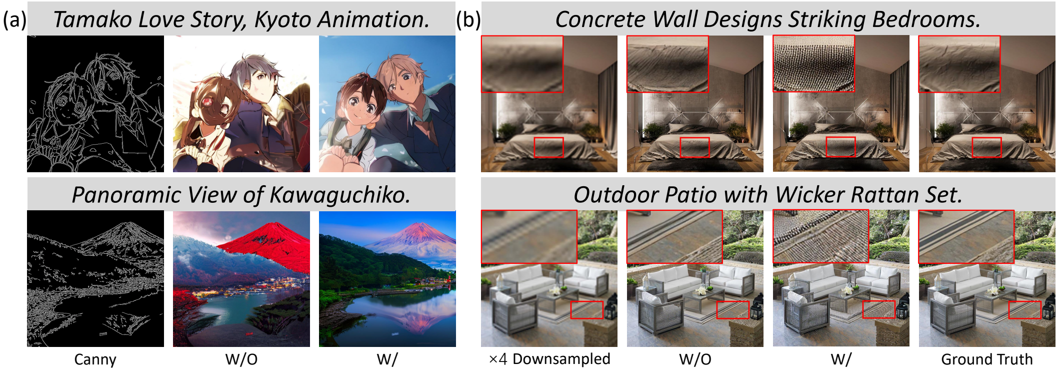
(a)
Tamako Love Story, Kyoto Animation.
Panoramic View of Kawaguchiko.
Canny
W/O
W/
(b)
Concrete Wall Designs Striking Bedrooms.
Outdoor Patio with Wicker Rattan Set.
×4 Downsampled
W/O
W/
Ground Truth

Figure 13: Comparison of UniCon adopting cross attention blocks in Adapter with (a) Canny and (b) downsampled images.

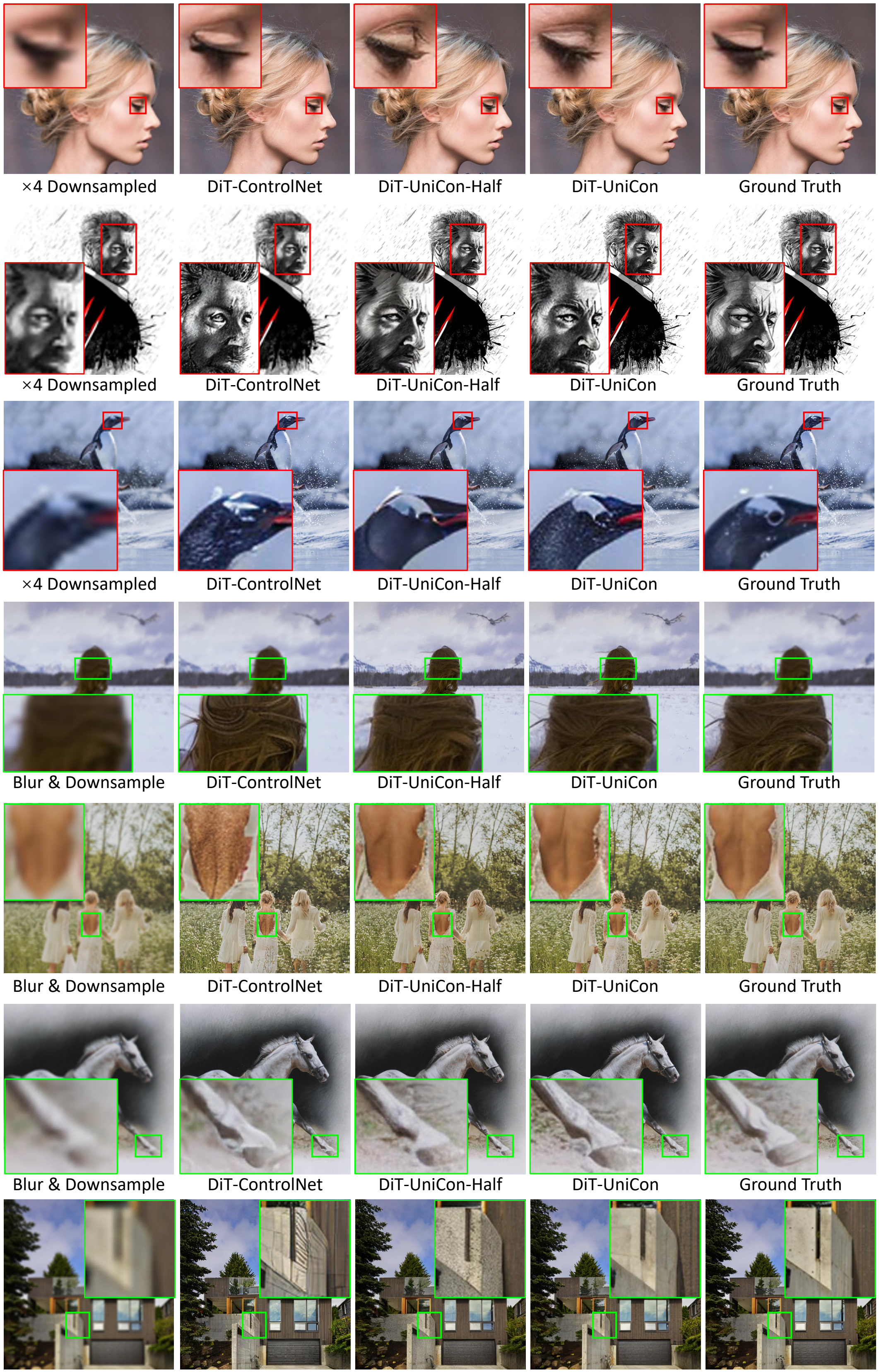

Figure 14: Qualitative comparison of DiT with ControlNet (Zhang et al., 2023) and UniCon dealing with downsampled image condition.

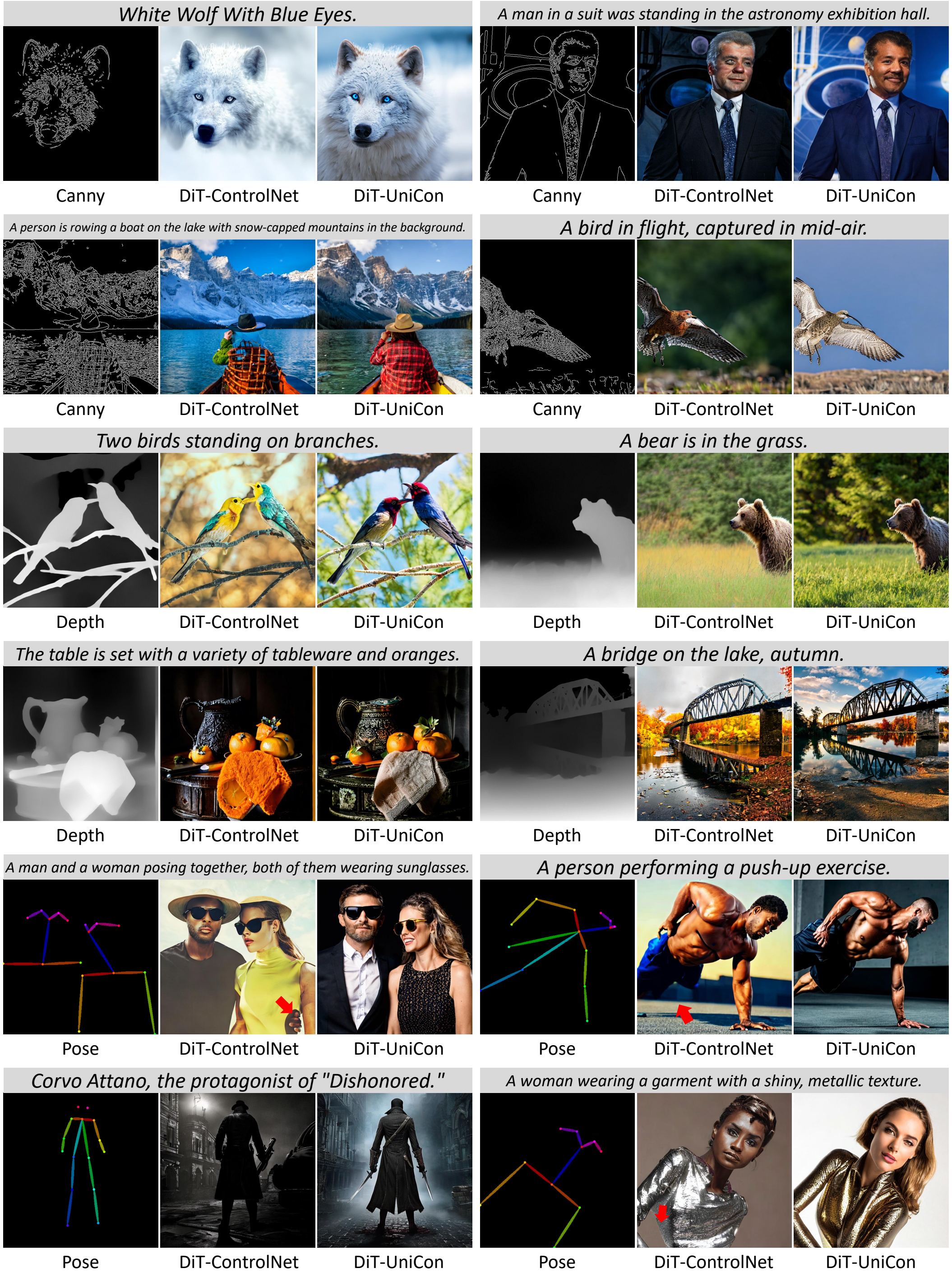
White Wolf With Blue Eyes.
Canny
DiT-ControlNet
DiT-UniCon
A man in a suit was standing in the astronomy exhibition hall.
Canny
DiT-ControlNet
DiT-UniCon
A person is rowing a boat on the lake with snow-capped mountains in the background.
Canny
DiT-ControlNet
DiT-UniCon
A bird in flight, captured in mid-air.
Canny
DiT-ControlNet
DiT-UniCon
Two birds standing on branches.
Depth
DiT-ControlNet
DiT-UniCon
A bear is in the grass.
Depth
DiT-ControlNet
DiT-UniCon
The table is set with a variety of tableware and oranges.
Depth
DiT-ControlNet
DiT-UniCon
A bridge on the lake, autumn.
Depth
DiT-ControlNet
DiT-UniCon
A man and a woman posing together, both of them wearing sunglasses.
Pose
DiT-ControlNet
DiT-UniCon
A person performing a push-up exercise.
Pose
DiT-ControlNet
DiT-UniCon
Corvo Attano, the protagonist of "Dishonored."
Pose
DiT-ControlNet
DiT-UniCon
A woman wearing a garment with a shiny, metallic texture.
Pose
DiT-ControlNet
DiT-UniCon

Figure 15: Qualitative comparison of DiT with ControlNet (Zhang et al., 2023) and UniCon dealing with canny, depth, and pose image conditions.

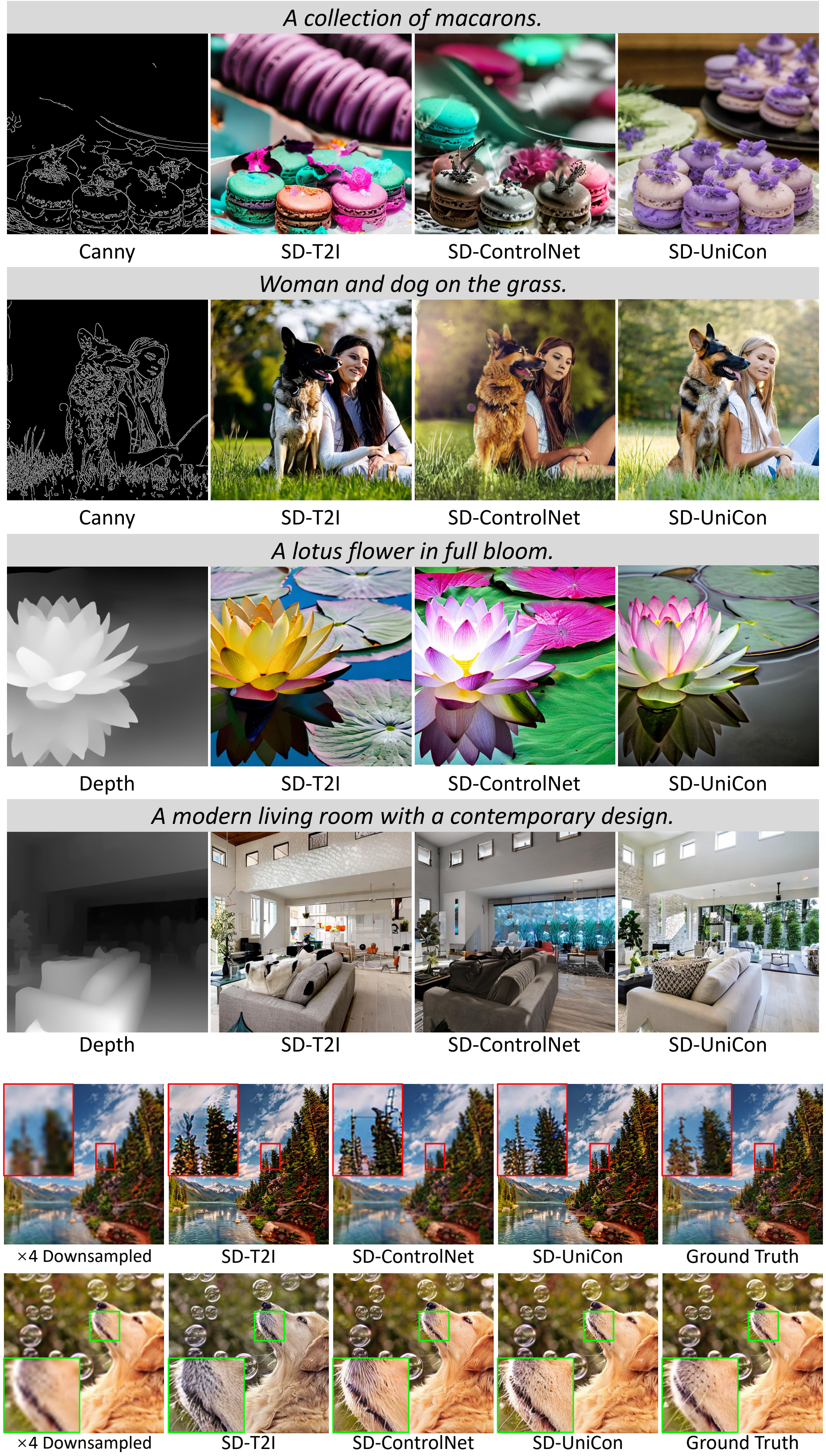

Figure 16: Qualitative comparison of SD with T2I-Adapter (Mou et al., 2024), ControlNet (Zhang et al., 2023) and UniCon dealing with canny, depth, and downsampled image conditions.

Task	Adapter	Unidirectional	Controller	Connector	Controllability			Generation Quality				Text Consistency
			CrossAttn	Type	PSNR↑	SSIM↑	LPIPS↓	FID↓	CLIP-IQA↑	MAN-IQA↑	MUSIQ↑	CLIP-Score↑
Canny	Encoder	✗	✓	ZeroMLP	-	0.4748	0.3280	51.52	0.6439	0.1861	65.24	0.7724
	Skip-Layer	✗	✓	ZeroMLP	-	0.4983	0.3033	49.78	**0.6629**	0.1978	66.05	0.7776
		✓	✓	ZeroMLP	-	0.5078	0.3016	56.93	0.6224	0.1737	63.66	0.7561
	Decoder	✗	✓	ZeroMLP	-	0.5131	0.2953	59.32	0.6047	0.1621	62.51	0.7507
		✓	✓	ZeroMLP	-	0.5343	0.2714	55.22	0.6347	0.1780	64.27	0.7612
		✓	✗	ZeroMLP	-	0.5260	0.2798	56.16	0.6177	0.1638	62.40	0.7520
		✓	✓	ShareAttn	-	0.5236	0.2778	56.22	0.6154	0.1723	63.75	0.7606
		✓	✓	ZeroFT	-	0.5426	0.2658	52.31	0.6563	0.1906	66.32	0.7696
	Full	✗	✓	ZeroFT	-	0.5053	0.3070	50.17	0.6397	0.1867	64.70	0.7818
		✓	✓	ZeroFT	-	**0.5458**	**0.2538**	**46.71**	0.6577	**0.2029**	**66.45**	**0.7889**
DS	Encoder	✗	✓	ZeroMLP	34.82	0.9352	0.0650	26.43	0.7147	0.2459	69.37	0.7996
	Skip-Layer	✗	✓	ZeroMLP	35.49	0.9385	0.0616	24.99	0.7229	0.2541	**70.00**	0.8009
		✓	✓	ZeroMLP					Failed			
	Decoder	✗	✓	ZeroMLP	34.85	0.9417	0.0589	25.84	0.6979	0.2325	68.26	0.8013
		✓	✓	ZeroMLP	35.59	0.9478	0.0519	23.55	0.7036	0.2358	68.61	0.8018
		✓	✗	ZeroMLP	35.67	0.9495	0.0502	22.99	0.7012	0.2499	69.23	0.8013
		✓	✗	ShareAttn	35.55	0.9486	0.0510	23.03	0.7078	0.2481	69.24	0.8012
		✓	✗	ZeroFT	35.64	0.9512	0.0475	22.07	0.7042	**0.2675**	69.51	0.8025
	Full	✗	✗	ZeroFT	36.53	0.9475	0.0522	23.04	0.7212	0.2609	69.91	**0.8026**
		✓	✗	ZeroFT	**37.34**	**0.9542**	**0.0453**	**20.34**	**0.7251**	**0.2831**	69.99	0.8022

Table 7: Results of full ablation study. ↑ indicates the larger the better and ↓ indicates the lower the better. **Bold** and underline represent the best and second best performance.

Algorithm 1 Pseudo Code for One Round Training Cost Evaluation

```
Require: sampled noise (eta), noised input (xt), timestep (t), prompt (y), condition (c)
device = torch.device(0)
model = model.to(device)
WEIGHT_MEMORY = torch.cuda.max_memory_allocated(device)
with torch.no_grad():
    pred_eta = model(xt, t, y, c)
    _ = MSE_Loss(pred_eta, eta)
ACTIVATION_MEMORY = torch.cuda.max_memory_allocated(device)
pred_eta = model(xt, t, y, c)
loss = MSE_Loss(pred_eta, eta)
loss.backward()
GRADIENT_MEMORY = torch.cuda.max_memory_allocated(device)
fp_start_time = time.time()
pred_eta = model(xt, t, y, c)
loss = MSE_Loss(pred_eta, eta)
FP_TIME = time.time() - fp_start_time
bp_start_time = time.time()
optimizer.zero_grad() loss.backward()
optimizer.step()
BP_TIME = time.time() - bp_start_time
OPTIMIZER_MEMORY = torch.cuda.max_memory_allocated(device)
return *_MEMORY, *_TIME
```

Algorithm 2 Pseudo Code for DiT-ControlNet Forward Pass

```
Require: noised input (xt), timestep (t), prompt embedding (y), condition (c)
x = base_model.image_embedding(xt)
t_emb = base_model.timestep_embedding(t)
c = controller.image_embedding(c)
t_emb_cond = controller.timestep_embedding(t)
x = x + c
for base_block, control_block in zip(base_model.blocks, controller.blocks) do
    x = base_block(x, t_emb)
    c = control_block(c, t_emb_cond)
    x = x + control_block.connector(c)
end for
pred = base_model.proj_out(x)
return pred
```

Algorithm 3 Pseudo Code for DiT-UniCon Forward Pass

```
Require: noised input (xt), timestep (t), prompt embedding (y), condition (c)
with torch.no_grad():
    x = base_model.image_embedding(xt).detach()
    t_emb = base_model.timestep_embedding(t).detach()
c = controller.image_embedding(c)
t_emb_cond = controller.timestep_embedding(t)
c = c + x
for base_block, control_block in zip(base_model.blocks, controller.blocks) do
    with torch.no_grad():
        x = base_block(x, t_emb).detach()
    c = control_block(c, t_emb_cond)
    c = c + control_block.connector(x)
end for
pred = controller.proj_out(c)
return pred
```